

ARTICLE OPEN



Inhibition of the CEBP β -NF κ B interaction by nanocarrier-packaged Carnosic acid ameliorates glia-mediated neuroinflammation and improves cognitive function in an Alzheimer's disease model

Wang Yi-Bin^{1,3}, Li Xiang^{1,3}, Yang Bing^{1,3}, Zhang Qi^{1,3}, Jiao Fei-Tong², Wang Minghong², Zhang Xiangxiang¹, Kang Le¹, Li Yan¹, Sui Ping¹, Gao Yufei¹, Xu Ye²✉ and Wang Chun-Yan^{1,2}✉

© The Author(s) 2022

Neuroinflammation occurs early in Alzheimer's disease (AD). The initial stage of AD is related to glial dysfunction, which contributes to impairment of A β clearance and disruption of synaptic connection. CEBP β , a member of the CCAAT-enhancer-binding protein (CEBP) family, modulates the expression of inflammation-associated genes, and its expression is elevated in brains undergoing degeneration and injured brains. However, the mechanism underlying CEBP β -mediated chronic inflammation in AD is unclear. In this study, we observed that increases in the levels of nuclear CEBP β facilitated the interaction of CEBP β with the NF κ B p65 subunit, increasing the transcription of proinflammatory cytokines in the APP/PS1 mouse brain. Oral administration of nanocarrier-packaged carnosic acid (CA) reduced the aberrant activation of microglia and astrocytes and diminished mature IL-1 β , TNF α and IL-6 production in the APP/PS1 mouse brain. CA administration reduced β -amyloid (A β) deposition and ameliorated cognitive impairment in APP/PS1 mice. We observed that CA blocked the interaction of CEBP β with NF κ B p65, and chromatin immunoprecipitation revealed that CA reduced the transcription of the NF κ B target genes TNF α and IL-6. We confirmed that CA alleviated inflammatory mediator-induced neuronal degeneration and reduced A β secretion by inhibiting the CEBP β -NF κ B signalling pathway in vitro. Sulfobutyl ether-beta-cyclodextrin (SBE β CD) was used as the encapsulation agent for the CA-loaded nanocarrier to overcome the poor water solubility and enhance the brain bioavailability of CA. The CA nanoparticles (NPs) had no obvious toxicity. We demonstrated a feasible SBE β CD-based nanodelivery system targeting the brain. Our data provide experimental evidence that CA-loaded NPs are potential therapeutic agents for AD treatment.

Cell Death and Disease (2022)13:318; <https://doi.org/10.1038/s41419-022-04765-1>

INTRODUCTION

Alzheimer's disease (AD), the most common cause of dementia, has become one of the most critical global public health issues with the ageing of the population; however, effective interventions are still lacking due to the complexity of the mechanisms underlying AD, including central and peripheral dysfunction. Cytokine dysregulation is considered to play key roles in AD [1, 2]. It has been found that interleukin (IL)-1 β [3], IL-6 [4] and transforming growth factor (TGF)- β [5] accumulate around β -amyloid (A β) plaques in the AD brain postmortem. A series of clinical studies have indicated that neuroinflammation occurs early in AD [6, 7]. Glial dysfunction occurs in the initial stage of AD [8]. Senescent glia produces more inflammatory cytokines [9]. An imbalance between pro- and anti-inflammatory cytokines is present in the CSF and serum of mild cognitive impairment (MCI) or AD patients. There are significant increases in the levels of

proinflammatory cytokines, such as IL-1 β , IL-6, and tumour necrosis factor (TNF)- α , and decreases in the levels of anti-inflammatory cytokines, such as the IL-1 receptor antagonist IL-10 [7]. IL-1 β elevation can further facilitate the production of IL-6, which may result in an increase in the level of hyperphosphorylated tau, the major component of intracellular neurofibrillary tangles (NFTs) [10]. Moreover, systemic immune challenges triggered by inflammatory inducers can lead to A β accumulation and gliosis [11]. In addition, phosphorylated tau can directly bind to the cytokine CX3CL1 receptor, which may provoke microglia, leading to tau internalisation by microglia and the spreading of tau hyperphosphorylation [12].

The incidence of AD is notably decreased among patients with rheumatoid arthritis treated with long-term nonsteroidal anti-inflammatory drug (NSAID) therapy [13, 14], although clinical trials of NSAIDs for AD treatment with small sample sizes failed to

¹Institute of Health Sciences, Key Laboratory of Medical Cell Biology of Ministry of Education, China Medical University, Shenyang 110122, China. ²Translational Medicine Laboratory, School of Basic Medical Sciences, Jilin Medical University, Jilin 132013, China. ³These authors contributed equally: Wang Yi-Bin, Li Xiang, Yang Bing and Zhang Qi. ✉email: xuye_9707@163.com; wangchunyan@cmu.edu.cn

Received: 23 December 2021 Revised: 10 March 2022 Accepted: 25 March 2022

Published online: 07 April 2022

provide the expected outcomes [15, 16]. The inconsistency of these findings is probably due to the fact that these anti-inflammatory agents target generic components rather than particular inflammatory molecules associated with AD [17]. Butchart and colleagues obtained positive results when using TNF α inhibitors to treat AD [18]. Targeting the imbalance between pro- and anti-inflammatory cytokines in AD by regulating the homeostasis of cytokines and proinflammatory genes is a potential therapeutic strategy for AD, and targeting the upstream modulators of cytokines is an attractive approach [18].

The roles of the transcription factor CEBP β , a member of the CCAAT-enhancer-binding protein (CEBP) family, have attracted increasing attention in regulating cytokine-mediated inflammatory responses. The binding sites in the regions of the CEBP β promoter and enhancer endow the transcription factor with the ability to regulate a number of cytokines and proinflammatory genes [19]. CEBP β modulates IL-1 β production in macrophages in vitro [20]. Papin and colleagues observed that CEBP β is an essential regulator that confers cell responsiveness to TNF α [21]. CEBP β knockdown alleviates the expression of proinflammatory genes and reduces the neurotoxic effects of activated microglia [22]. Inhibition of CEBP β ameliorates glial activation and the neuroinflammatory response in a rat model of Parkinson's disease [23]. Interestingly, CEBP interacts with NF κ B. The C-terminus of the Rel homology domain of NF κ B can bind with the bZIP region of CEBP, enhancing the transcription of inflammatory genes by NF κ B [24]. Importantly, CEBP β expression in the cortex is markedly increased in specimens from AD patients compared with those from nondemented elderly individuals at autopsy [25]. The transcript levels of *Cebpb* are higher in the brains of aged AD transgenic mice than in the brains of age-matched controls [26]. Downregulating *Cebpb* gene expression ameliorates Tau pathology and cognitive dysfunction in an AD mouse model [27]. Targeting CEBP β intervention might be a potential therapeutic strategy for mitigating the neuronal damage triggered by inflammation in neurodegenerative diseases.

Carnosic acid (CA), also named (4aR,10aS)-5,6-dihydroxy-7-isopropyl-1,1-dimethyl-1,3,4,9,10,10a-hexahydro-2H-phenanthrene-4a-carboxylic acid, a phenolic diterpene isolated from rosemary, has attracted increasing attention because of its pharmacologic properties. Through its antiadipogenic activity, CA plays role in inhibiting colon tumour formation [28]. CA can inhibit inflammation and joint destruction in an animal model of arthritis by reducing the levels of TNF α , IL-1 β and IL-6 [29]. Interestingly, CA-mediated decreases in glucose levels and diabetic nephropathy remission are involved in inhibition of NF κ B [30]. An analogue of CA, Carnosol, could mitigate ROS-mediated bone loss, which was involved in the regulating on NF κ B [31]. Oxidative stress and inflammation are linked. Inflammation could interact with oxidising agents, triggering oxidative stress. Accordingly, oxidative stress facilitates the release of inflammatory cytokines [32]. It is reasonable to speculate that CA may play a neuroprotective role in modulating the CEBP β -NF κ B-cytokine network in AD.

In this study, we investigated the effects of CA treatment on pro- and anti-inflammatory cytokine homeostasis and the potential effects of CA on CEBP β target genes and molecular pathways in the treatment of AD. The lipophilicity and poor water solubility of CA and the feasibility of delivering CA to the brain should be considered. Furthermore, the acceptance of oral noninvasive therapy is high, but the first-pass effect of the liver and the influence of the gastrointestinal environment on drugs should also be considered. Here, we developed a sulfobutyl ether-beta-cyclodextrin (SBE β CD)-based nanoparticles (NPs) drug carrier that can deliver CA to the brain. We observed that CA suppressed CEBP β transcriptional activity and reduced the interaction between CEBP β and NF κ B in the brains of APP/PS1 Tg mice. CA-mediated decreases in CEBP β expression inhibited amyloidogenesis. Our results reveal the therapeutic effects of CA on the CEBP β

network and show that CA might be a promising therapeutic agent for the treatment of AD.

MATERIALS AND METHODS

Preparation of SBE β CD and CA-SBE β CD NPs

SBE β CD (1.05 g) was dissolved in 5 mL of double-distilled water. The solution was then added to 1.0 mL of Tween 80, 10.0 mL of 10% poloxamer 407 and 2.0 mL of polyethylene glycol 400. After vortexing, the emulsion was used as the solvent for SBE β CD nanoparticles (SBE β CD NPs). The pH was adjusted to 7.2 using trihydroxymethyl aminomethane. SBE β CD NPs containing CA (purity, 99.034%; Shanghai Winherb Medical Science Co., Ltd., Shanghai, China), namely, CA-SBE β CD NPs, were prepared as follows: CA (0.24 g) was dissolved in 0.8 mL of 100% ethanol. Under continuous magnetic stirring, CA-ethanol solution was gradually added to the SBE β CD inclusion complex (IC) (drug-SBE β CD molar ratio, 1:1) [33] at room temperature, and the total volume was adjusted to 40.0 mL with deionized water. After ultrasonication (500 W, 3 s interval, 15 min), the formed NPs were filtered through a 0.22- μ m microporous membrane.

Characterisation of the NP system

Size distribution, surface charge and morphology of the NPs. The particle size and zeta potentials were measured by laser diffraction or Doppler velocimetry at 25 °C with a Zetasizer Nano ZS90 instrument (Malvern Instruments Ltd., Malvern, Worcestershire, UK). All measurements were conducted at least three times.

After negative staining using 1% phosphotungstic acid, the morphology of the NPs was examined with a transmission electron microscope (TEM) (JEM-2100, Nikon, Japan) at an accelerating voltage of 200 kV.

Encapsulation and loading efficiency assays. CA-SBE β CD NPs were assessed by high-performance liquid chromatography (HPLC). Briefly, to separate the free CA from the CA-SBE β CD NPs, 5 mg of lyophilised NPs containing CA were dissolved in 1 mL of dichloromethane. The organic phase was then collected and extracted using 5 mL of ethanol. After centrifugation, the supernatants were filtered with a microporous membrane for HPLC. The chromatographic conditions were as follows: Phenomenex C18 analytical column (150 mm \times 4.6 mm, 5 micron particle size); mobile phase, acetonitrile-0.1% phosphoric acid (55:45, v/v); column temperature, 25 °C; flow rate, 1.0 mL/min; and injection volume, 20 μ L. The encapsulation efficiency (EE) and loading efficiency (LE) were calculated as follows:

$$\text{Encapsulation efficiency (\%)} = \frac{\text{mass of the CA} - \text{unbound CA}}{\text{mass of the CA}} \times 100$$

$$\text{Loading efficiency (\%)} = \frac{\text{mass of the CA} - \text{unbound CA}}{\text{mass of the nanoparticles}} \times 100$$

Hydrogen nuclear magnetic resonance (1 H-NMR) spectroscopy. The chemistry of the NP system was evaluated with a 1 H-NMR spectrometer (Bruker AVANCE III HD 500 MHz, Switzerland). Chloroform-d (deuteriochloroform, CDCl $_3$) was used as the solvent. Hydrogen spectrum data were analysed and plotted with MestReNova combined with Origin software.

In vitro drug release analysis. Dynamic dialysis was performed to assess CA release from the CA-SBE β CD NPs. Briefly, 2 mL of CA-SBE β CD NPs was transferred into a cellulose-based dialysis tube (molecular weight cut-off: 14,000 Da) that had been pre-soaked in distilled water. The tube was closed tightly, placed into an oscillator containing 50 mL of 0.01 M phosphate-buffered saline (PBS, pH 7.4 and pH 6.0) and gently shaken at 100 rpm (37 °C). Five millilitres of the medium was assessed at the indicated times (0.25, 0.5, 1, 2, 4, 6, 8, 10, 24, 48 and 72 h), and an equal volume of PBS at the same temperature was added at each sampling time. The amount of CA in the sample at each time point was determined by HPLC according to the chromatographic conditions above, and the cumulative release percentage was calculated.

Safety evaluation of the NPs. To assess the cytotoxicity of the nanosystem in vitro, the NP system was administered to human neuroblastoma SH-SY5Y cells. SH-SY5Y cells were routinely plated in 96-well plates in Dulbecco's modified Eagle's medium (DMEM) containing 10% heat-inactivated foetal bovine serum (FBS), 100 U/mL penicillin and 100 μ g/mL streptomycin in a fully humidified incubator with 5% CO $_2$ at 37 °C. The cells

were maintained in serum-free DMEM until they reached 80% confluence. Two hours later, the cells were exposed to *SBE β CD NPs*, *CA-SBE β CD NPs* and *CA* as indicated. Untreated cells were used as matched controls. Cell viability was determined by the cell counting kit-8 (CCK-8) assay. The absorbance was measured at 450 nm using a 96-well plate reader.

To assess acute toxicity *in vivo*, two-month-old male C57BL/6 mice (body weight: 20–22 g), were randomly divided into three groups: orally gavaged with saline, *SBE β CD NPs* or *CA-SBE β CD NPs* ($n = 8$ in each group) every day for 7 days. Animal usage was in accordance with the guidelines established by the Ministry of Health, Peoples Republic of China and the ethical standards for laboratory animals of China Medical University. On the 8th day, the mice were sacrificed. The stomach, jejunum, ileum and colon of each mouse were collected and fixed in 4% paraformaldehyde for 48 h at 4 °C. After dehydrated, 10- μ m sections of the tissues were prepared with a freezing microtome. The sections were mounted onto slides and stained with haematoxylin and eosin (H&E).

To evaluate chronic toxicity, male C57BL/6 mice ($n = 8$ in each group) were gavaged with the above-mentioned solutions for 30 days. The body weight of the mice was monitored each day. On day 31, the heart, liver, spleen, lung and kidney were removed. After fixation and dehydration, the samples were sectioned at a thickness of 10 μ m and stained with H&E. The operators were blinded to the group allocation during the experiments.

Assessment of the BBB permeability of NPs *in vitro*. Transwell assays were performed to evaluate the ability of the NPs to cross the blood-brain barrier (BBB) and target neuronal cells. Briefly, hCMEC/D3 cells were loaded in the upper chamber of a Transwell system (Corning, NY, USA). The cells were cultured in DMEM containing 10% heat-inactivated FBS, 1% L-glutamic acid and 5 μ M 2-mercaptoethanol in a fully humidified incubator with 5% CO₂ (37 °C). SH-SY5Y cells were seeded in the bottom chamber. The SH-SY5Y cells were cultured in the same manner as hCMEC/D3 cells, but the culture medium was supplemented with 100 U/mL penicillin and 100 μ g/mL streptomycin. The medium of both cell types was replenished each day. The transendothelial electrical resistance (TEER) was monitored on consecutive days. After they formed a tight confluent monolayer, the hCMEC/D3 cells in the upper chamber were treated with 6 μ M 6-coumarin (Cou6) suspension, nanoemulsion (NE)-dissolved Cou6 or Cou6-tagged *SBE β CD NPs* for 24 h. The SH-SY5Y cells in the bottom chamber were collected and analysed by flow cytometry (FCM).

Evaluation of Cou6-loaded NP localisation *in vivo*. To investigate the retention and localisation of the drug delivery system, C57BL/6 mice were gavaged with Cou6-loaded *SBE β CD NPs* or NE-dissolved Cou6 (60 mg/kg). After 90 min, the mice were anaesthetised with pentobarbital sodium salt (70 mg/kg) by intraperitoneal injection and sacrificed by decapitation. The liver, kidney and brain of each animal were collected and cut into frozen sections (10 μ m), and fluorescence was assessed using a confocal laser scanning microscope (Nikon 1, Japan).

Mice and treatment. Male APP/PS1 (B6C3-Tg [APP^{swe}, PSEN1^{dE9}] 85Dbo/Mmjax) double Tg mice (RRID: MMRRC_034829-JAX) and age-matched C57BL/6 mice were obtained from Jackson Laboratory. All animal experimental procedures were approved by the Ethics Committee of China Medical University. Four-month-old mice were randomly assigned to three treatment groups: the group treated with vehicle control (*SBE β CD NPs*), the group treated with *CA-SBE β CD NPs* at a dose of 10 mg/kg *CA* and the group treated with *CA-SBE β CD NPs* at a dose of 30 mg/kg *CA* ($n = 8$ in each group). The mice were given the indicated treatment by oral gavage once *per day* for 5 months. The body weights of the mice were recorded, and the general behaviours of the mice were monitored daily.

Analysis of cognition. To investigate affiliative social behaviour, the nest construction test was conducted. The mice were housed individually in cages with 1-cm-deep corncob bedding one day before the test. Eight pieces of paper (5 cm \times 5 cm) were neatly placed on the bedding to introduce nesting conditions. The nesting behaviour of each mouse was observed the following morning. The nests constructed from the pieces of paper were photographed for seven consecutive days. The nesting scores of the mice were determined according to a four-point scoring system: (1) the paper was not obviously bitten or torn and was randomly scattered; (2) the paper was gathered in a corner or on the side of the cage but not obviously bitten or torn; (3) the paper was gathered in a corner or on the side of the cage and showed moderate biting or tearing; (4) the paper was gathered in a corner or on the side of the cage and showed extensive biting or tearing.

To evaluate the recognition memory of the mice, the novel object recognition test (NORT) was performed. Briefly, the mice were allowed to habituate to the arena (50 cm length \times 50 cm width \times 40 cm height) and the testing room for 10 min twice a day for 2 days. On the next day, two plastic blocks of the same volume were placed in the arena. Each mouse was given 5 min to explore the blocks. Then, the mouse was placed back in its cage for 5 min, after which it was subjected to a 5-min short-term memory (STM) test. During the STM test, the mouse was placed in the arena after one of the objects was replaced with a novel plastic cylinder. For the long-term memory (LTM) assessment, the familiar or novel objects were replaced, and the interval was 24 h. The exploratory behaviour was defined as when a mouse directed its nose toward an object within a range of 2 cm and/or directly touched the object with its nose and/or forepaws. The discrimination index was calculated as the percentage of time spent exploring the novel object compared to the total time spent exploring both objects.

To investigate the spatial learning and memory of the mice, the Morris water maze (MWM) test was conducted. The test involved 8 days of testing. The mice were allowed to swim in a tank of water. First, the mice underwent 2 days of training in which a visible platform was present in the tank. Then, the mice underwent the navigation test, in which they searched for a hidden platform 1 cm below the water surface, for 5 days. The mice were subjected to three tests, each of which lasted a maximum of 60 s, at a 60-s intertrial interval. The escape latency was recorded using an overhead video tracking system. Finally, on the 8th day, the platform was removed from the tank, and a probe trial was carried out to evaluate the search bias of the mice. The times of each mouse crossed the region in which the platform had previously been located and the distances travelled in this region were recorded.

Preparation of tissue samples. Twenty-four hours after the behavioural tests, the mice were deeply anaesthetized using sodium pentobarbital (60 mg/kg, intraperitoneally). After transcardial perfusion with pre-cooled 0.9% saline, the animals were sacrificed by decapitation. The mouse brains were sagittally cut in half. The right hemisphere of each mouse was fixed, dehydrated and cut into frozen sections for morphological analyses. The left hemisphere of each mouse was used to isolate cells or snap-frozen in liquid nitrogen and stored at 80 °C for biochemical assays.

Cell culture and treatment. Human glioblastoma A172 cells were cultured in DMEM/F12 (Life Technologies) containing 10% FBS and 1% penicillin/streptomycin. Human neuroblastoma SH-SY5Y cells were obtained from ATCC (ATCC[®] CRL2266[™]), which were authenticated (underwent STR analysis, sterility test and Human pathogenic virus testing) and tested for mycoplasma contamination. Cells stably transfected with the human β -amyloid precursor protein Swedish mutation (APP^{swe}) or empty vector (*neo*) were grown in DMEM/F12 containing 10% FBS and 1% penicillin/streptomycin and supplemented with 200 μ g/mL G418. When the cells reached 80% confluence, they were cultured in DMEM/F12 without serum, penicillin/streptomycin or G418. lipopolysaccharide (LPS), a major outer surface membrane component of all gram-negative bacteria, was administered to A172 cells to trigger proinflammatory responses. The cells were then incubated with *CA*, or a lentivirus expressing CEBP β as indicated.

FCM. To assess the degree of mitochondrial membrane polarisation, cultured cells were labelled with 2 μ M of JC-1 (MitoProbe[™] JC-1 Assay Kit) for 20 min at 37 °C and protected from light. The JC-1 Green (FL1) and JC-1 Red (FL2) signals were quantified using detectors. The ratio of JC-1 red fluorescence signal to JC-1 green fluorescence signal was determined.

For apoptosis evaluation, cells isolated from the prefrontal cortex of the brains were harvested by centrifugation at 400 \times g, trypsinized, and resuspended in PBS. Cells isolated from the tissue specimens or cultured cells were then fixed in pre-cooled 75% ethanol for 1 h. Apoptotic cells were quantified with an Annexin V-fluorescein isothiocyanate (FITC)/propidium iodide (PI) apoptosis detection kit according to the manufacturer's instructions. Briefly, the cells were treated with binding buffer (5 μ L Annexin V-FITC and 5 μ L PI) for 15 min at room temperature in the dark. The samples were analysed by FCM. Apoptosis was quantified using FITC (FL1) and PI (FL2) fluorescence detectors. At least three independent experiments were performed.

Immunostaining. Frozen mouse brains were cut coronally into ten-micrometre-thick sections. The sections were rehydrated in 0.01 M PBS and treated with 3% hydrogen peroxide to eliminate endogenous

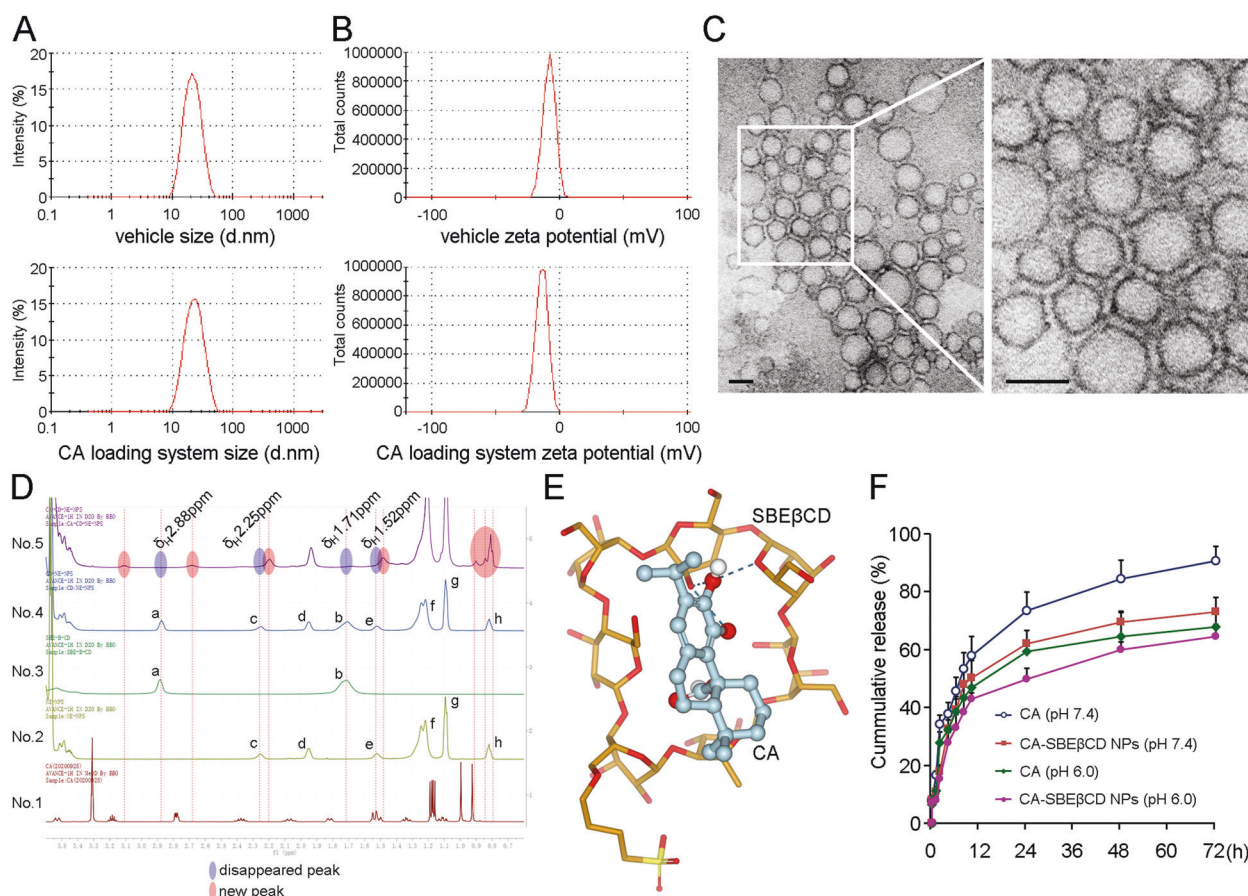


Fig. 1 Preparation and characterization of CA-SBE β CD NPs. The size distribution (A) and zeta potential (B) of SBE β CD NPs and CA-SBE β CD NPs were determined by laser light scattering. C The morphology of SBE β CD NPs was assessed by negative staining with sodium phosphotungstate solution and examined by transmission electron microscopy. Scale bar: 50 nm. D $^1\text{H-NMR}$ spectra of the components of CA-SBE β CD NPs. Resonance signals corresponding to the characteristic bonds of CA (No.1) appeared at 0.9–3.1 ppm. The characteristic peaks of SBE β CD (No.3) were at 2.88 and 1.71 ppm (peak a and b). NE (No.2), namely, nanoemulsions and auxiliary emulsion components without SBE β CD, presented signals at 2.55 ppm (peak c), 1.95 ppm (peak d), 1.52 ppm (peak e), 1.22 ppm (peak f), 1.09 ppm (peak g) and 0.83 ppm (peak h). The $^1\text{H-NMR}$ spectrum of SBE β CD NPs (No.4) exhibited peaks in similar regions as SBE β CD and NE because the NPs contained SBE β CD and NE groups. Compared with CA-SBE β CD NPs, new peaks at chemical shifts of 0.80 to 1.00 ppm and 1.45 to 1.55 ppm appeared in the $^1\text{H-NMR}$ spectrum of CA-SBE β CD NPs (No.5). Obvious increases in peak intensity at 1.15–1.35 ppm in the resonance signals of CA-SBE β CD NPs confirmed the synthesis of a link between CA and SBE β CD, and the signal peaks disappeared at 2.88 and 1.71 ppm suggests a bonding reaction between SBE β CD and CA. E Molecular docking diagram. CA potentially interacts with SBE β CD through hydrogen bonds: a hydroxyl group of CA respectively forms two intermolecular hydrogen bonds with the hydroxyl group and oxygen atom of SBE β CD; and a hydroxyl group of CA forms a hydrogen bond with a hydroxyl group of SBE β CD. The binding affinity was -21.35 kJ/mol. F CA release from CA-SBE β CD NPs in PBS at pH 7.4 or 6.0 in vitro. CA dissolved in NE was used as control.

peroxidase activity. The samples were rinsed and then blocked with 5% normal donkey serum for 30 min at room temperature. The sections were incubated with a primary antibody for immunohistochemistry (IHC) or a mixture of primary antibodies for double immunofluorescence (IF) for 16 to 18 h in a humidified chamber at 4 °C. After being thoroughly rinsed, the sections for IHC were incubated with an appropriate biotinylated secondary antibody at room temperature for 2 h and then treated with streptavidin peroxidase for 30 min. After being rinsed, the samples were stained with 0.025% 3,3'-diaminobenzidine plus 0.0033% H_2O_2 in 0.1 M Tris-HCl buffer (pH 7.4) for 5 min. The sections were then dehydrated, cleared and covered with neutral balsam. The slices were examined, and images were captured with an optical microscope equipped with a digital camera (Olympus). For double IF staining, the slices were incubated with a mixture of appropriate fluorescence-conjugated secondary antibodies for 2 h at room temperature and protected from light. After being thoroughly washed, nuclear chromatin was visualised using 4',6-diamidino-2-phenylindole (DAPI). The sections were mounted with an anti-fading mounting medium and scanned using a confocal laser scanning microscope.

Sandwich enzyme-linked immunosorbent assay (ELISA). The A β level in the APP/PS1 mouse brain was measured using human A β 1–40 and human A β 1–42 ELISA kits (Invitrogen) according to the manufacturer's protocol.

Briefly, the mouse cortex samples were lysed in ice-cold 20 mM Tris-HCl (pH 8.5) or 50 mM Tris-HCl containing 5 M guanidine HCl (pH 8.0) to analyse the contents of soluble A β and insoluble A β , respectively. The absorbance was measured at 450 nm using a 96-well plate reader.

IL-1 β , IL-6 and TNF α secretion into the supernatants of the cultured cells was respectively measured with the commercial V-PLEX Human IL-1 β kit, IL-6 ELISA kit and TNF α ELISA kit (Meso Scale Discovery), according to the manufacturer's instructions. The absorbance was measured at a wavelength of 450 nm.

To measure DNA binding activity, nuclear extracts were obtained from the cultured cells using a nuclear extraction kit (Active Motif, Inc., Carlsbad, CA) according to the manufacturer's instructions. The DNA binding activity of NF κ B was examined with a TransAM ELISA kit (Active Motif).

Western blot assays. Protein was extracted from cells or tissue homogenates using RIPA buffer (pH 8.0) supplemented with a protease inhibitor cocktail. The protein concentration was measured using a BCA protein assay kit. Twenty-microgram of protein was loaded on sodium dodecyl sulfate polyacrylamide gels to separate the proteins. The separated proteins were then transferred onto polyvinylidene fluoride (PVDF) membranes (Millipore, Temecula, MA, USA), which were probed with the primary antibodies listed in Supplementary Table S1. After being rinsed,

the PVDF membranes were incubated with appropriate HRP-conjugated secondary antibodies. The immunoreactive bands were visualised with an enhanced chemiluminescence kit (Pierce, Rockford, IL, USA), and the band density was quantified with Quantity One software. Blots were repeated at least three times for every condition.

Immunoprecipitation. To immunoprecipitate endogenous proteins extracted from cells or brain homogenates, 2 micrograms of protein was incubated with commercial primary antibodies against CEBP β or control IgG for 16 h at 4 °C in a rotating incubator. The immune complexes were collected by incubation with True-Blot IP beads (eBioscience, Hatfield,

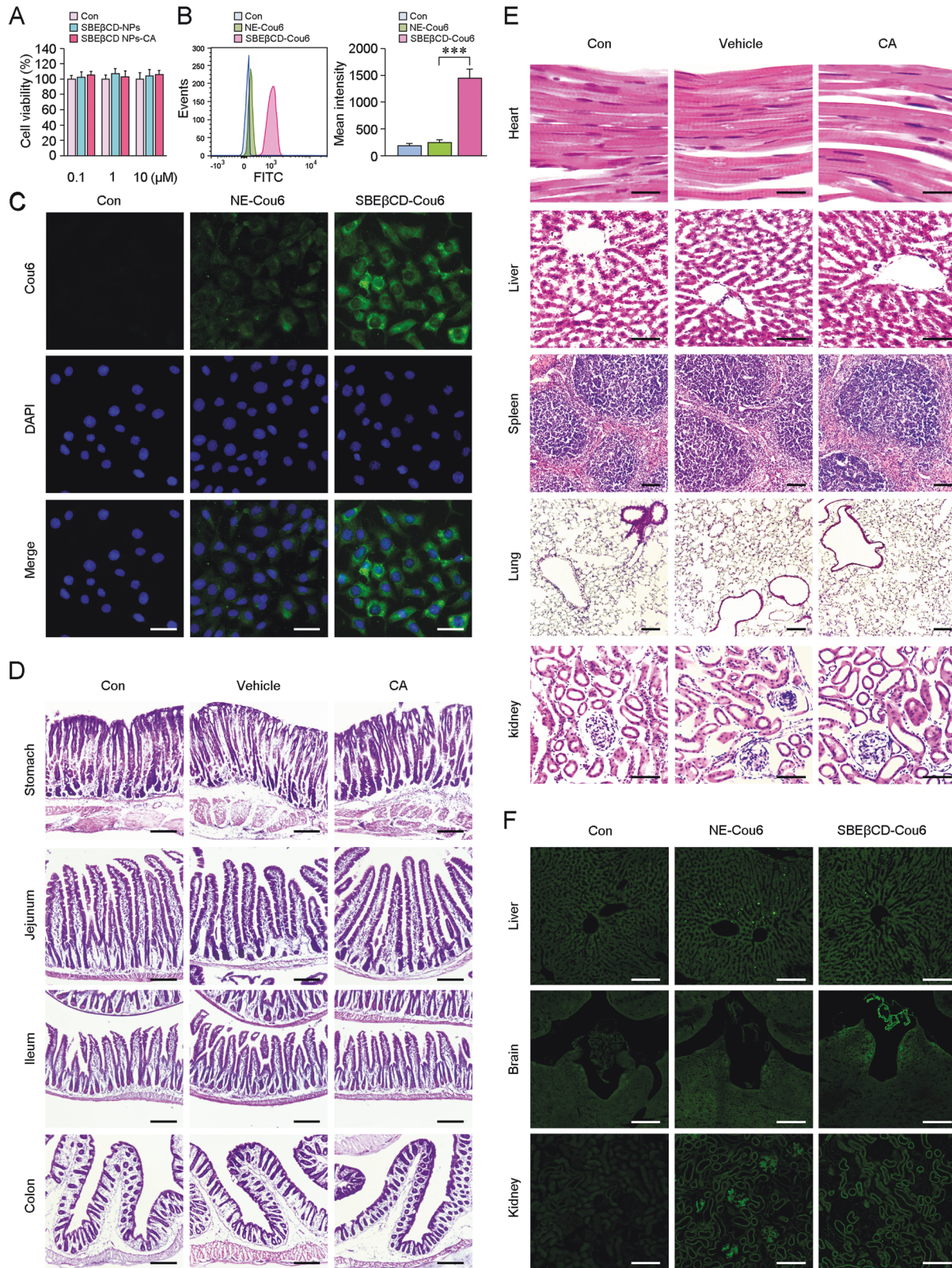


Fig. 2 Evaluation of the transport efficiency and biological safety of CA-SBE β CD NPs. **A** In vitro cytotoxicity of SBE β CD NPs, NEs without SBE β CD and CA-SBE β CD NPs. SH-SY5Y cell viability was measured using a CCK-8 kit. Untreated cells were used as the controls (Con). **B** A Transwell assay in which hCMEC/D3 cells were plated in the upper chamber and SH-SY5Y cells were plated in the lower chamber was conducted to assess the ability of the cells to cross the BBB. The fluorescence intensity was determined by FCM to assess the levels of Cou6 in SH-SY5Y cells cocultured with hCMEC/D3 cells, which were treated with Cou6 suspensions, NE-dissolved Cou6 (NE-Cou6) or Cou6-loaded SBE β CD NPs (SBE β CD-Cou6). Cells treated by Cou6 suspensions in DMEM were used as the controls (Con). **C** Localisation analysis by laser scanning microscopy showed marked green Cou6 fluorescence in the cytoplasm of SH-SY5Y cells. Representative images showing the fluorescence signals of Cou6 in SH-SY5Y cells cocultured with hCMEC/D3 cells treated with different NP formulations. Scale bars: 20 μ m. **D** H&E staining showing the morphology of stomach, jejunum, ileum and colon tissues from C57BL/6 mice orally gavaged with SBE β CD NPs or CA-SBE β CD NPs for 7 days. The tissue structure of the samples from each group was intact and the cells were neatly arranged. The connections between the cell layers were clear, and no obvious inflammatory cells were observed. Scale bars: 50 μ m. **E** Safety assessment of the chronic administration with SBE β CD NPs or CA-SBE β CD NPs to mice for 30 days. Heart, liver, spleen, lung and kidney sections were stained with H&E. The structures of tissue were clear and intact, and the cells were normally arranged. No inflammatory cell infiltration was observed. Scale bars: heart, 5 μ m; liver and kidney, 20 μ m; spleen and lung, 50 μ m. **F** Confocal laser scanning microscopy images showed the green fluorescence signals in the liver and kidney from the mice treated with NE-dissolved Cou6 and Cou6-loaded SBE β CD NPs. No fluorescence signals were observed in the brains of mice treated with NE-dissolved Cou6. Clear green Cou6 fluorescence were observed in the choroid plexus and periventricular region of the third ventricle from the brain sections of the mice administered with Cou6-loaded SBE β CD NPs. Scale bars: 50 μ m. *** p < 0.001 vs the NE-Cou6 groups by one-way ANOVA. Values are presented as the means \pm standard deviation (SD). All experiments were repeated at least three times.

United Kingdom) for another 2 h. The samples were rinsed with lysis buffer three times and eluted. Western blot analysis was performed with anti-NF κ B antibodies.

Real-time PCR. Total RNA was extracted from brain tissues or cultured cells using an RNA isolation kit according to the manufacturer's instructions. Two micrograms of total RNA from each sample was reverse transcribed using the Prime Script RT Reagent Kit. cDNA synthesis was performed at 37 °C for 15 min and 85 °C for 5 s. Quantitative real-time PCR was performed using SYBR Green PCR Master Mix on a 7300 Sequence Detection System. At least three independent analyses were conducted. The forward and reverse primers used for PCR are listed in Supplementary Table S2. The expression levels were calculated by normalising the cycle threshold (Ct) values to the total amount of β -actin. The expression levels in the treatment group are presented as a percentage of that in the control group.

Chromatin immunoprecipitation (ChIP). ChIP was performed as previously described [34]. Mouse brain tissues were fixed with 4% paraformaldehyde for 12 h at 4 °C and neutralised with 0.125 M glycine for 10 min at 4 °C. After being washed twice with precooled PBS containing protease inhibitor cocktail, the samples were homogenised with 0.1% SDS lysis buffer containing 0.5% Triton X-100, 150 mM NaCl, 20 mM Tris-HCl (pH 8.0) and protease inhibitor cocktail. The samples were then sonicated and collected. One-third of the nuclear proteins were used as genomic DNA controls, and the remaining proteins were incubated with antibodies against NF κ B for 18 h at 4 °C. Protein A-agarose beads were added to the reaction system and incubated with rotation for 1 h at 4 °C to capture the protein–DNA complexes. After being thoroughly rinsed, the specimens were collected by gentle centrifugation. The pellets were treated with elution buffer (pH 8.0), centrifuged and then treated with 5 M NaCl to reverse formaldehyde-induced crosslinking. After being heated for 12 h at 65 °C, the protein–DNA complexes were deproteinated with 20 mg/mL proteinase K for 1 h at 45 °C. The DNA samples were treated with phenol/chloroform and ethanol and amplified. Real-time PCR was carried out using primers for IL-6 and TNF α .

Lentiviral gene transfer of CEBP β . A lentivirus vector expressing CEBP β (LV-CEBP β) was produced for gene transfer as previously described [35]. Briefly, all lentiviral vectors were generated by transient transfection into HEK293 cells. Forty-eight hours after transfection, the viruses were harvested, purified and concentrated by ultracentrifugation. The viral titres were measured, and a stock virus solution with a titre of 10⁹ infectious U/mL was generated. After preliminary dose-response assays, SH-SY5Y cells were plated in DMEM containing 10% FBS at a density of 2 \times 10⁵ cells per cm² and infected with 1000 microlitres of stock virus in 1.9 millilitres of the medium. After infection for 12 h at 37 °C, the SH-SY5Y cells were incubated with fresh DMEM without serum for 24 h.

Statistical analysis. One-way, two-way or repeated-measures analysis of variance (ANOVA) was used to evaluate differences as appropriate. The effects of genotype and treatment and the effect of the genotype \times

treatment interaction were analysed. In all cases, two-sided P values less than 0.05 were considered significant.

RESULTS

Synthesis and characterization of the nanocarriers

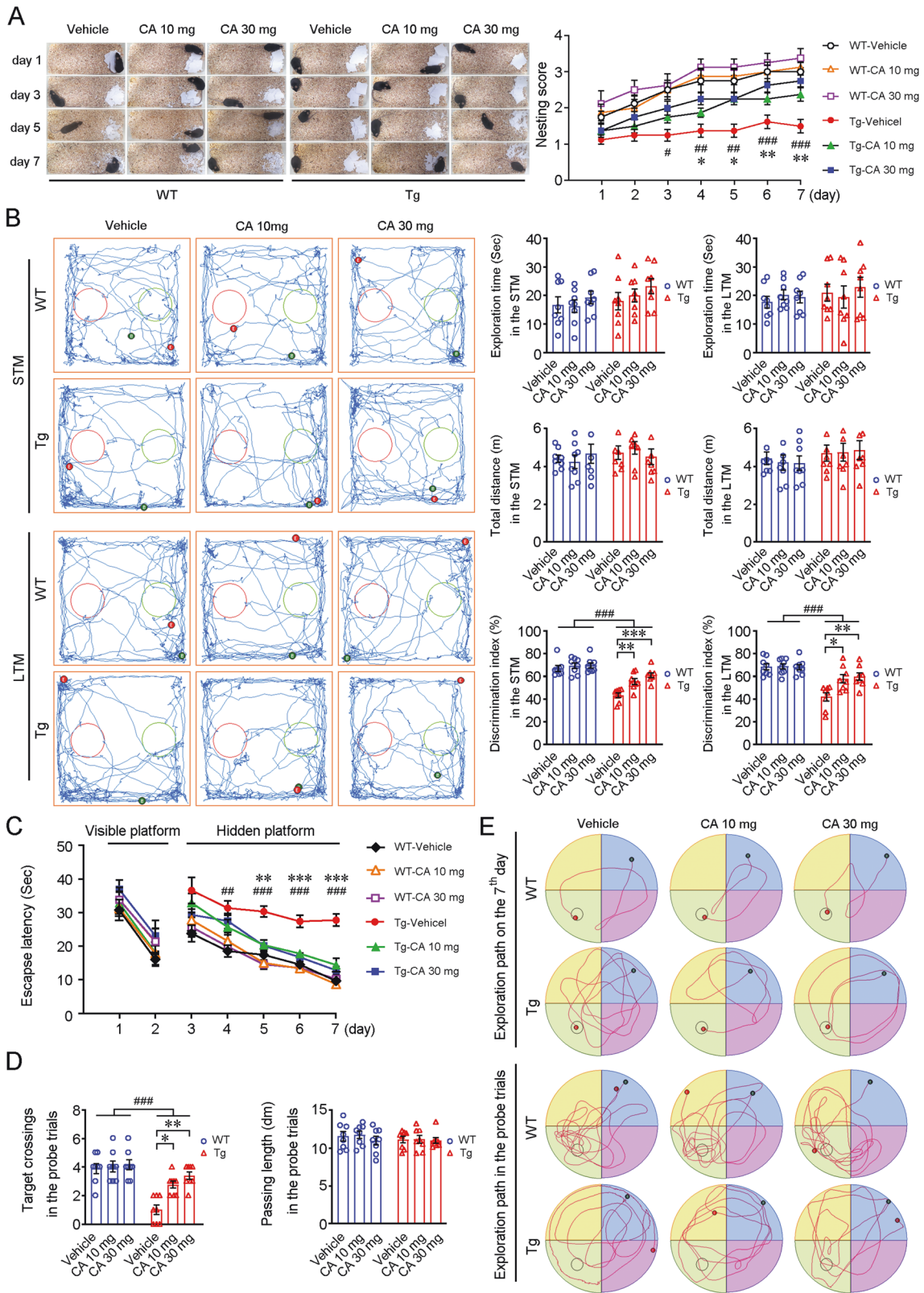
The internal cavity of SBE β CD is extended. The inclusion and dissolution rates of compound molecules of SBE β CD are higher than those of β -CD [36]. According to prior studies [33] and the EE and LE achieved in our study (Supplementary Table S3), SBE β CD and CA were prepared at a molar ratio of 1:1. Five percent (v/v) polyethylene glycol 400 (PEG 400) was used as the vehicle. The average particle sizes of the SBE β CD NPs and CA-SBE β CD NPs were 24.53 \pm 5.14 nm and 36.42 \pm 0.83 nm, respectively (Fig. 1A and Supplementary Table S3) and they had lower polydispersity indexes (PDIs) (0.243 \pm 0.093 and 0.264 \pm 0.004, respectively). The zeta potential of the SBE β CD NPs was -5.73 ± 2.12 mV, while that of the CA-SBE β CD NPs was -11.54 ± 1.45 mV (Fig. 1B and Supplementary Table S3). Transmission electron microscopy confirmed that the nanocarriers generally exhibited a regular spherical shape (Fig. 1C). The chemistry of the NPs was analysed by ¹H-NMR spectroscopy indicating that CA was successfully introduced into the nanocarrier system (Fig. 1D). Molecular docking assays (Supplementary Method S1) suggest that CA interacts with SBE β CD via hydrogen bonds (Fig. 1E).

The release of CA from the nanocarriers was examined at pH 7.4 and pH 6.0 (37 °C). Continuous CA release from CA dissolved in NE and CA-SBE β CD NPs were observed in the first 4 h at pH 7.4 and pH 6.0. After 4 h, the release of CA gradually slowed. Compared with that of CA from CA-NE, the cumulative release rate of CA from CA-SBE β CD NPs was relatively lower (Fig. 1F). CA-SBE β CD NPs also maintained sustained release at pH 6.0, demonstrating the relative stability of the release behaviour.

CA-SBE β CD NPs efficiently targets and enters the brain and is biologically safe according to preliminary studies

The in vitro cytotoxic effects of the nanocarrier system were investigated using SH-SY5Y cells. There were no significant differences in the viability of cells treated with nanocarriers containing 0.1–10 μ M CA and the viability of cells treated with other NPs (with or without equimolar concentrations of SBE β CD) (p > 0.05, Fig. 2A).

The efficiency of the nanocarriers in crossing the BBB was evaluated in hCMEC/D3 cells using the Transwell assay. As shown in Fig. 2B, higher fluorescence intensity was observed in SH-SY5Y cells cocultured with SBE β CD NPs-treated hCMEC/D3 cells in the upper chamber relative to that in SH-SY5Y cells cocultured with



NE-Cou6-treated hCMEC/D3 cells ($p < 0.001$). Localisation analysis by laser scanning microscopy showed significant green Cou6 fluorescence in the cytoplasm of SH-SY5Y cells cocultured with hCMEC/D3 cells plus Cou6-SBE β CD NPs. The fluorescence was granular and scattered (Fig. 2C).

To assess acute toxicity, stomach, jejunum, ileum and colon samples from each mouse orally gavaged with SBE β CD NPs (vehicle) or CA-SBE β CD NPs (CA) every day for 7 days were subjected to H&E staining. No, obviously abnormal status was observed among the groups (Fig. 2D). For chronic toxicity, a 30

Fig. 3 Evaluation of the effect of CA-SBE β CD NPs administration on the learning and memory of APP/PS1 mice. Four-month-old APP/PS1 (Tg) mice and age-matched C57BL/6 (WT) mice were orally gavaged with SBE β CD NPs (vehicle) or SBE β CD NPs loaded with 10 or 30 mg/kg CA for 5 months. **A** Representative images showing nests constructed by the mice. Nesting scores were quantified. **B** The recognition memory of WT and Tg mice was assessed by the NORT. The traces of the mice in the STM and LTM tests were recorded. The green dots and red dots respectively represent the starting and ending locations of the mice. Tg mice and WT mice showed similar total time and distance during the habituation phase. The discrimination index was used to compare the ability of the mice to recognise the familiar object. **C** Spatial learning and memory were evaluated by the MWM test. WT and Tg mice exhibited comparable escape latencies during the visible platform training phase. Tg mice performed longer escape latencies than WT mice in the hidden platform test from the 3rd day; CA treatment shortened the escape latency of Tg mice. **D** On the final day (the 8th day), the platform was removed, and the probe trial was performed. The number of times and the navigated distance of each mouse crossed the area in which the platform was previously located were quantified. **E** Representative traces show the exploration of the mice on the 7th and 8th day. * $p < 0.05$, ** $p < 0.01$, *** $p < 0.001$ vs vehicle-treated mice; # $p < 0.05$, ## $p < 0.01$ and ### $p < 0.001$ vs the WT mice by the repeated-measures ANOVA. Values represent the mean \pm standard error of the mean (SEM). $n = 8$ in each group.

days-administration above were performed. H&E staining showed no marked organ damage in the heart, liver, spleen, lung and kidney (Fig. 2E). To verify the transport efficiency of the nanocarriers *in vivo*, the fluorescence signals in brain sections were assessed by confocal laser scanning microscopy after oral administration of Cou6-labelled NPs (Fig. 2F).

CA-SBE β CD NPs treatment alleviates cognitive impairment in APP/PS1 mice

CA-SBE β CD NPs were orally administered to transgenic APP/PS1 mice (Tg) and age-matched wild-type (WT) C57BL/6 mice at a dose of 10 or 30 mg/kg beginning at 4 months of age. After 5 months of treatment, cognition was assessed. As shown in Fig. 3A, Tg mice exhibited deficits in nesting behaviour compared with the WT mice. The nesting scores of the CA-SBE β CD NPs (30 mg/kg CA)-treated Tg group were higher than those of SBE β CD NPs-treated Tg mice (vehicle controls) from the 4th day to the 7th day (Fig. 3A). The Tg mice presented poor recognition memory in the NORT (Fig. 3B). The discrimination index CA-SBE β CD NPs-treated Tg mice were higher than vehicle-treated Tg mice in the STM ($F(2,21) = 16.516$, $p < 0.001$) and LTM ($F(2,21) = 7.487$, $p < 0.01$) test. CA-SBE β CD NPs treatment markedly improved the spatial learning ability of the Tg mice by shortening the escape latency during the hidden platform test (Fig. 3C, E) and increasing the frequency without altering total distances during the probe trial (Fig. 3D, E) in the in MWM test.

CA-SBE β CD NPs treatment mitigates AD-like pathology in the brains of APP/PS1 mice

Immunohistochemical staining showed that fewer A β plaques were observed in the CA-treated Tg mice than in those of vehicle-treated Tg mice ($ps < 0.001$, Fig. 4A, B). Furthermore, ELISA assays showed that the levels of soluble A β 42 and A β 40 were significantly reduced after CA treatment ($ps < 0.001$, Fig. 4C). TdT-mediated dUTP nick end labelling (TUNEL) staining showed that apoptosis cells were less in the brains of CA-treated Tg mice than in those of vehicle-treated Tg mice (Fig. 4D, E). We investigated the protein levels of synaptophysin (SYN, a presynaptic vesicle protein), synapsin 1 (a synaptic vesicle-related protein) and PSD-95 (a postsynaptic density protein) by immunoblotting. As shown in Fig. 4F, CA treatment alleviated the decline of these protein levels ($ps < 0.001$) in the Tg mice. CA treatment also affected the protein expression of SYN ($F(2,21) = 5.547$, $ps < 0.05$) and synapsin 1 ($F(2,21) = 12.847$, $ps < 0.001$) in the hippocampi of the WT mice.

CA-SBE β CD NPs administration alleviates the abnormal aggregation of glia in the brains of APP/PS1 mice

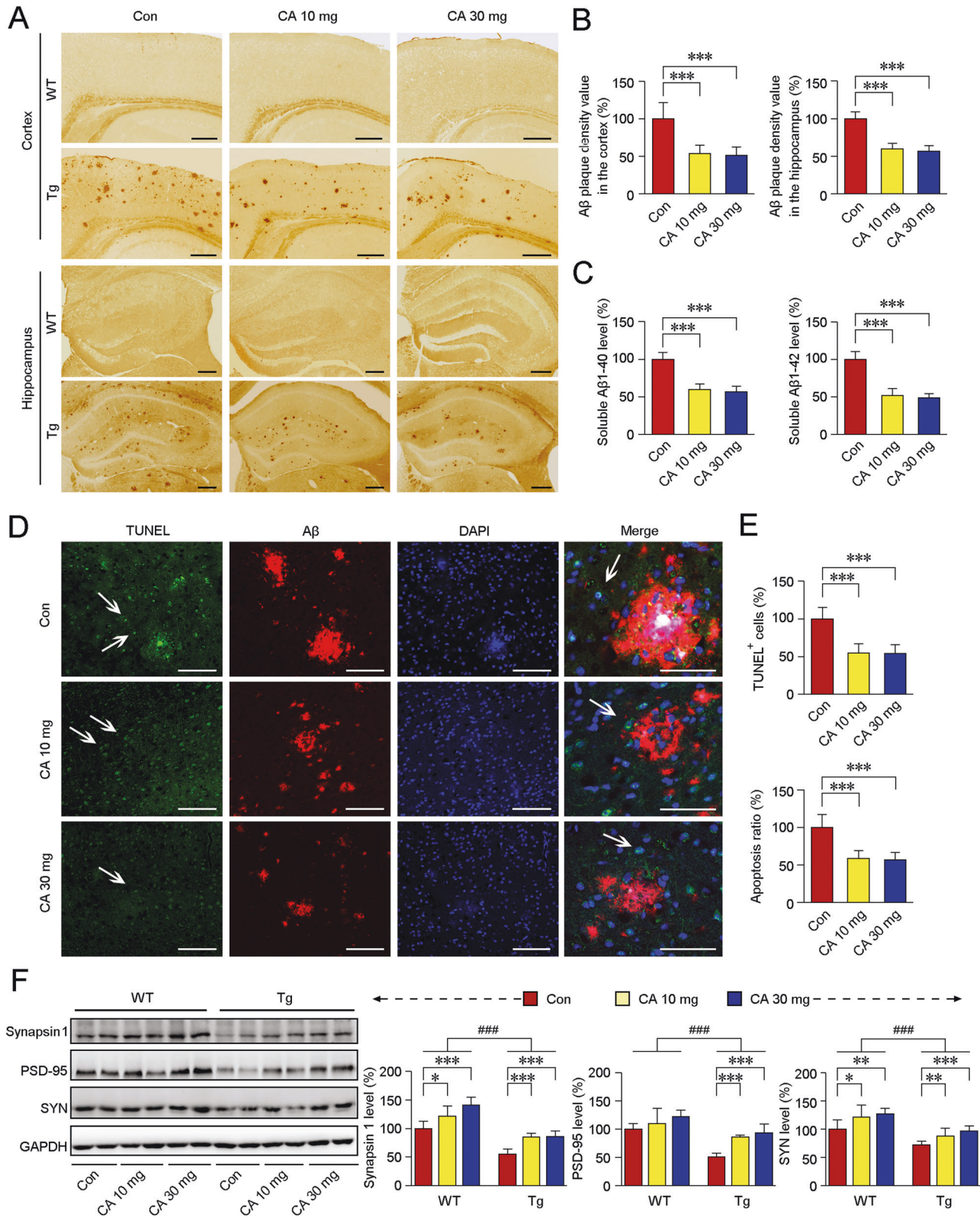
Considering the anti-inflammatory properties of CA and the deleteriousness of inflammation in promoting aberrant synaptic pruning and facilitating A β pathology [37], we investigated the effects of CA-SBE β CD NPs treatment against neuroinflammation.

As shown in Fig. 5A, B, the immunostaining signals of GFAP, an astrocyte marker, were increased in the brains of Tg mice than those of WT mice ($F(1,30) = 274.485$, $p < 0.001$). CA-SBE β CD NPs treatment alleviated the accumulation of astrocytes in the Tg mice brains. The intensity of GFAP around A β plaques in the CA-treated Tg mice was reduced compared with that in the vehicle-treated Tg mice (Fig. 5C, E). Moreover, the intensity of Iba1 immunoreactivity around A β plaques was markedly attenuated under CA treatment in the Tg mice brains (Fig. 5D, E). The protein expression of GFAP, Iba1 and CD11b (a microglial marker) was determined by Western blot analysis, and the observed changes in expression were consistent with above-mentioned changes caused by CA-SBE β CD NPs treatment (Fig. 5F).

CA-SBE β CD NPs administration reduces the release of IL-1 β , IL-6 and TNF α and diminishes the interaction of CEBP β with NF κ B in the APP/PS1 mouse brain

Neuroinflammation, even in the earliest stages, induces the release of proinflammatory factors and leads to neuronal injury [17]. As shown in Fig. 6A, the protein levels of mature IL-1 β ($F(1,30) = 101.522$, $p < 0.001$), TNF α ($F(1,30) = 87.968$, $p < 0.001$) and IL-6 ($F(1,30) = 40.036$, $p < 0.001$) were increased in the brains of Tg mice than those of WT mice. CA-SBE β CD NPs treatment diminished the protein levels above in the brains of both genotypes without altering pro-IL-1 β protein levels ($ps > 0.05$). The mRNA levels of TNF α ($F(1,30) = 39.083$, $p < 0.001$, Fig. 6B) and IL-6 ($F(1,30) = 40.036$, $p < 0.001$, Fig. 6C) were higher in the brains of Tg mice than those of WT mice. CA-SBE β CD NPs treatment suppressed the gene expression of TNF α and IL-6 in both genotypes ($ps < 0.001$).

To elucidate the effects of CA on regulating inflammatory signals, we analysed the expression of NF κ B. CA management relieved the increases of protein levels in both nuclear- and cytosolic NF κ B p65 subunit in the Tg mice brains (Fig. 6D, $ps < 0.001$). The effects of CA treatment on NF κ B mRNA levels were as well ($ps < 0.001$, Fig. 6E). We examined the expression of COX-2, a downstream target of NF κ B involved in the inflammatory process. The elevations of COX-2 protein expressions in the Tg mice brains were suppressed by CA-SBE β CD NPs treatment ($ps < 0.01$). It has been reported that IL-1 β -related NLRP3 expression is involved in NF κ B activation [38]. In the present study. The increases of NLRP3 protein expression in the Tg mice brains were mitigated under CA-SBE β CD NPs treatment. CEBP β is a critical regulator of IL-6 production [26], and CEBP β is essential for regulating IL-1 β and TNF α secretion [39]. CEBP β acts upstream of NF κ B p65, modulating the maturation of IL-1 β [20]. The interactions of NF κ B with CEBP β enhance the transcriptional activity of NF κ B [24]. In our study, CA-SBE β CD NPs treatment alleviated the elevation in both CEBP β protein expressions (Fig. 6D) and CEBP β mRNA levels (Fig. 6F) in the Tg mice. IF double labelling of CEBP β with GFAP (Fig. 6G) or Iba1 (Fig. 6H) showed the CEBP β expression and its relationship with astrocytes and microglia in the hippocampi of the mice.



To investigate whether the CA-induced decrease in CEBP β expression could modulate the interaction of CEBP β with NF κ B, we examined the CEBP β -NF κ B p65 complex by coimmunoprecipitation (Co-IP). As shown in Fig. 6I, CA treatment relieved the

increases of CEBP β -NF κ B p65 interactions in the Tg mice brains. Meanwhile, ChIP assays showed that CA administration mitigated the elevation of NF κ B recruitment to TNF α (Fig. 6J) and IL-6 (Fig. 6K) in the Tg group ($p < 0.001$).

Fig. 4 Effects of CA-SBE β CD NPs treatment on AD-related pathology in the APP/PS1 mouse brain. **A** A β -positive senile plaques were detected in APP/PS1 (Tg) mice and age-matched C57BL/6 (WT) mice treated with CA-SBE β CD NPs (loaded with 10 or 30 mg/kg of CA) or SBE β CD NPs (vehicle control) for 5 months. **B** The A β plaque density in the cerebral cortex and hippocampus was quantified. **C** Soluble A β 40 and A β 42 levels in the cortex were measured by ELISA. **D** Confocal laser scanning microscopy images showing apoptosis around A β -positive areas. TUNEL staining (green) showing apoptotic cells around A β plaques (red). DAPI was used to label the nuclei (blue). Scale bars: 100 μ m. The white arrows indicate apoptotic cells. The high-magnification images in the right panels show the localisation of apoptotic cells around the A β -positive deposits. Scale bar = 60 μ m. **E** Quantification of the apoptotic cells. **F** Western blot analysis showing the expression of the synaptic proteins, synapsin 1, PSD-95 and SYN. Blots were repeated at least three times for every condition. * p < 0.05, ** p < 0.01 and *** p < 0.001 vs vehicle-treated mice by the one-way ANOVA (A–E). * p < 0.05, ** p < 0.01, *** p < 0.001 vs vehicle-treated mice; ### p < 0.001 vs the WT mice by the two-way ANOVA with post hoc Fisher's least significant difference (LSD) tests. Values represent the mean \pm SD. n = 8 in each group.

CA provides neuroprotection and attenuates neuroinflammation by regulating CEBP β /NF κ B

It has been demonstrated that silencing CEBP β alleviates glial activation and reduces dopaminergic damage in a Parkinson's disease model [23]. Based on some of the common molecular mechanisms of neurodegeneration, we investigated whether CA-induced CEBP β inhibition is related to modulations of the glial cascade and exerts neuroprotective effects in an AD cell model in vitro. As shown in Fig. 7A, the LPS-triggered elevations of TNF α (p < 0.001), mature IL-1 β (p < 0.01) and IL-6 (p < 0.01) protein levels were attenuated by CA treatment, and the effects of CA on the IL-1 β , IL-6 and TNF α secretions in the medium of LPS-primed A172 cells were as well (ps < 0.001, Fig. 7B). CA treatment mitigated LPS-induced increases of CEBP β (p < 0.01) and NF κ B (p < 0.001) in the nuclei, and COX-2 protein expressions in the cytoplasm (p < 0.05) (Fig. 7C). Meanwhile, CA treatment diminished the upregulation of nuclear NF κ B and COX-2 expressions (Fig. 7D), alleviated mitochondrial lesions (Fig. 7E) and diminished apoptosis (Fig. 7F) in the *neo* and APPsw cells incubated with LPS-primed cell-condition medium. CA treatment also mitigated the increases of A β 40 and A β 42 secretions in *neo* and APPsw cells treated with the conditioned medium (Fig. 7G).

Interactions of NF κ B with BACE1 enhanced the transactivation of BACE1 [40], facilitating the amyloidogenic pathway. Considering the role of CEBP β as the upstream regulator of NF κ B [20], we investigated the specificity of CA for suppressing the transcriptional activity of NF κ B and verified that CA downregulated BACE1 expression via the CEBP β /NF κ B signalling pathway. We delivered CEBP β to SH-SY5Y cells using a lentiviral vector-encoding human CEBP β (LV-CEBP β). As shown in Fig. 8A, CA treatment mitigated the LV-CEBP β pretreatment-caused increases of nuclear NF κ B p65 protein levels in the SH-SY5Y cells (p < 0.01). CA addition ameliorated LV-CEBP β -triggered increases of NF κ B DNA binding activity (Fig. 8B, p < 0.01). IF staining of NF κ B p65 confirmed those results above (Fig. 8C). FCM analyses showed that LV-CEBP β -treated cells exhibited the highest intracellular fluorescence intensity for NF κ B p65 and CEBP β (ps < 0.001). By contrast, CA addition diminished LV-CEBP β -caused increases of NF κ B p65 and CEBP β expressions (Fig. 8D, ps < 0.01). Co-IP assays indicated that CA treatment relieved LV-CEBP β -induced elevation of CEBP β -NF κ B interactions (p < 0.01, Fig. 8E). The protein levels of nuclear NF κ B p65 and BACE1 were reduced after treatment with CA or an NF κ B activation inhibitor, JSH-23 (20 μ M for 6 h); however, these effects were diminished by LV-CEBP β treatment (ps < 0.001, Fig. 8F). Furthermore, we observed that administration of an NF κ B activator, phorbol myristate acetate (PMA, 30 ng/mL for 6 h), blocked the CA-induced decreases in BACE1 and NF κ B protein expressions (ps < 0.01, Fig. 8G).

DISCUSSION

Inflammatory alterations occur prior to the appearance of A β plaques [41]. During 'inflammageing', cytokine network dysfunction is associated with ageing and age-related diseases [42]. As critical components of the innate immune system in the central

nervous system, microglia and astrocytes, produce cytokines and perform monitoring [43]. IL-1 β secretion at physiological doses by microglia is required for long-term potentiation (LTP) induction, learning and memory formation [44]. A low dose of TNF α can regulate synaptic function by modulating AMPA receptor levels, synaptic strength and homeostatic plasticity [45]. However, ageing is related to increased and persistent inflammation [42]. Astrocytes and microglia take on opposite roles with age, as they increase the production of proinflammatory cytokines and reduce the production of anti-inflammatory cytokines [46]. Chronic inflammation is a common occurrence in ageing and AD [47]. A sustained inflammatory response is observed in the brains of AD patients [3]. Sustained activation of microglia weakens their capacity to bind and phagocytose A β and decreases A β degradation [48]. However, microglia still produce proinflammatory cytokines [49]. Importantly, a high level of IL-1 β impairs LTP and hinders learning and memory in a dose-dependent manner [44].

NF κ B signalling pathway plays important role in cellular responses to neuronal injury and synaptic plasticity in the central nervous system [50]. NF κ B modulates immunity by regulating the transcription of cytokines and immune response genes. In response to stimuli, NF κ B translocates from the cytosol to the nucleus to induce the transcription of target genes [51]. Importantly, NF κ B signalling is directly associated with spinogenesis and strengthens synapse connections during learning and memory formation [52]; however, NF κ B activation in neurons of the aged brain was shown to be incredibly toxic [53]. Sustained activation of NF κ B is consistent with the chronic inflammation observed in areas of the brain undergoing atrophy [54]. Activated NF κ B is clearly observed in neurodegenerating cells of post-mortem brains of AD patients [55]. A β neurotoxicity is dependent on NF κ B during gliosis [56]. In contrast, blocking NF κ B lessened IL-1 β -induced degeneration [57]. Disrupting the binding of NF κ B to the promoter of *Bace1* suppresses inflammatory processes [58]. NF κ B inhibition is considered a potential target for reducing neuroinflammatory damage and thus ameliorating AD.

Some natural products, such as polyphenols [59] and alkaloids [60], can alleviate AD-related lesions by inhibiting NF κ B signalling pathways. In vivo experiments showed that CA can suppress NF κ B activation and alleviate high fat diet-induced brain injury in mice [61]. Interestingly, CA is considered a neuroprotective agent due to its anti-inflammatory and mitochondrial protective effects [62]. In our study, CA treatment alleviated the elevation of protein expression of nuclear NF κ B p65 in the Tg mice brains. Similarly, CA treatment downregulated the protein and mRNA levels of the inflammatory biomarkers IL-6, TNF α and COX-2, suggesting that CA-induced inhibition of NF κ B nuclear translocation suppresses downstream inflammation-related signals. Moreover, CA treatment significantly reduced LPS-primed cell apoptosis and diminished A β 42 and A β 40 secretion in vitro; these findings are similar to those of a previous study [63]. The relationship between CEBP β and NF κ B initially received attention because of its regulatory effects on IL-6 [64] and IL-1 β [20]. In CEBP β -null mice, the expression of proinflammatory genes and the neurotoxicity caused by activated microglia are mitigated [22]. CEBP β protein

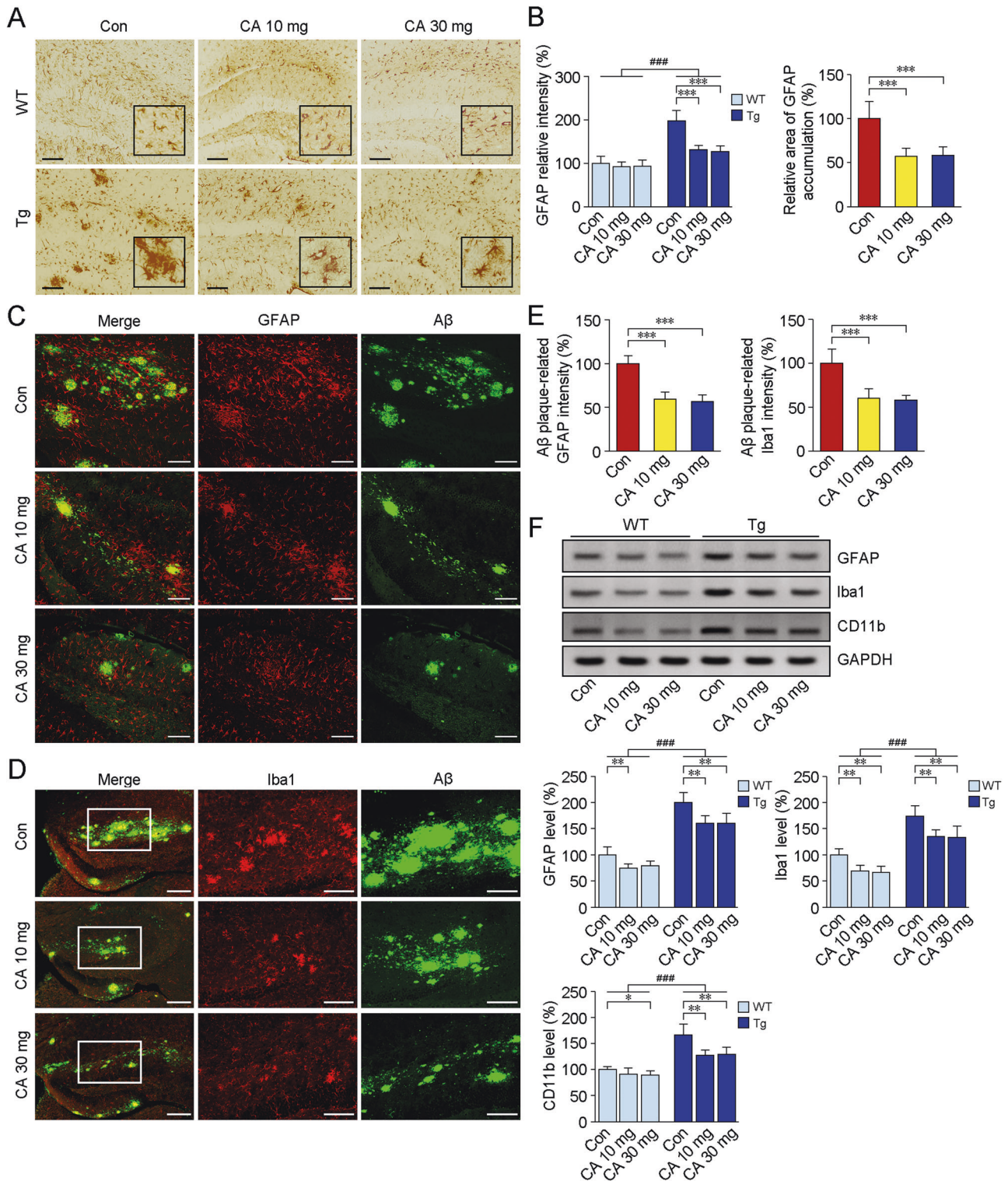
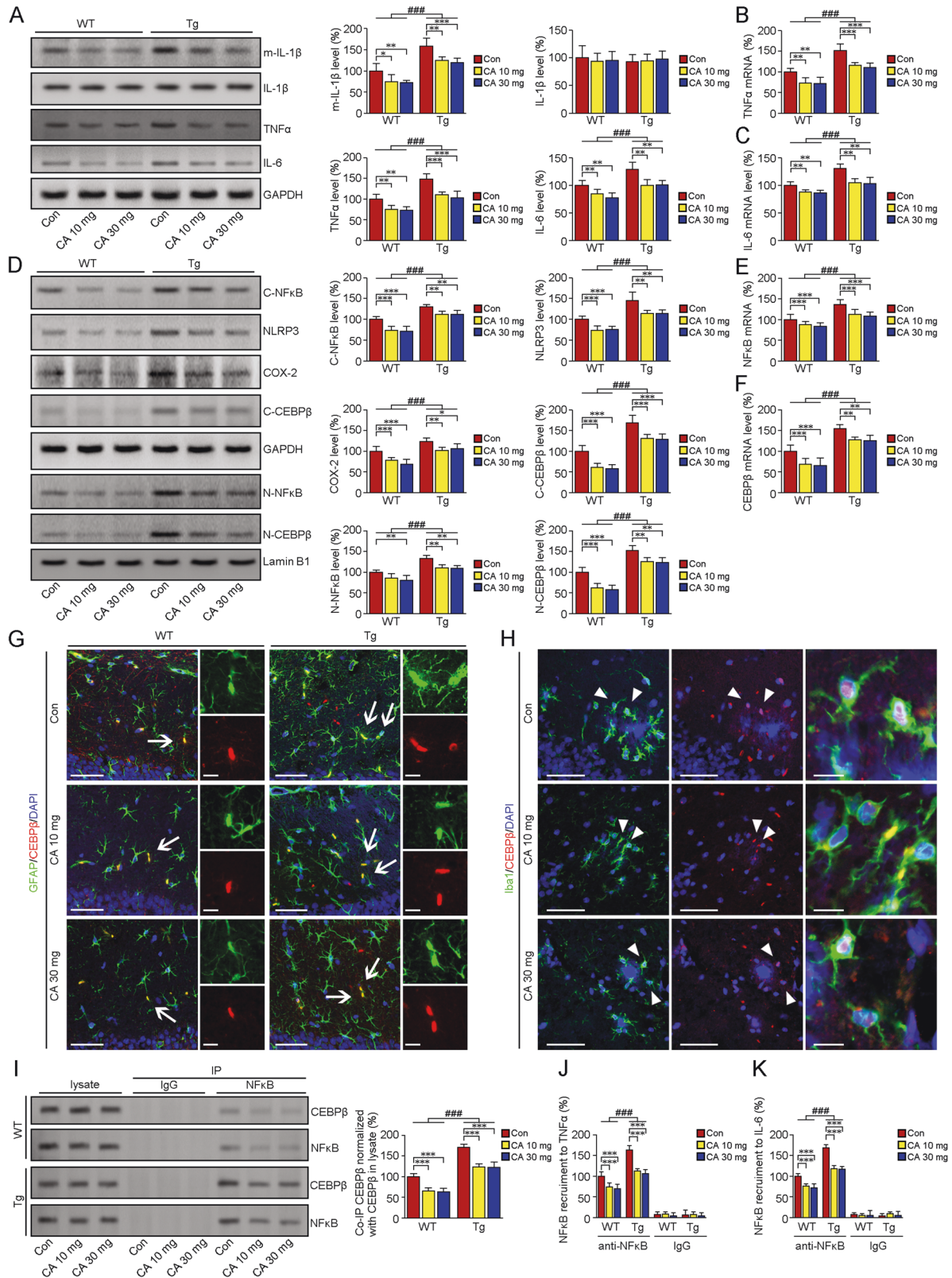


Fig. 5 Effects of CA-SBEβCD NPs treatment on microglial and astrocyte activation in the brains of APP/PS1 mice. APP/PS1 Tg mice and age-matched WT C57BL/6 mice were administered with CA-SBEβCD NPs (loaded with 10 or 30 mg/kg CA) or SBEβCD NPs (vehicle control) for 5 months. **A** Astrocytes in the hippocampus were detected by IHC with an anti-GFAP antibody. In the brains of Tg mice, astrocytes aggregated and exhibited somatic hypertrophy and thickening of the primary processes. Scale bars: 200 μm. **B** Quantification of the GFAP intensity in WT and Tg mice. **C** Representative confocal laser scanning microscopy images showing the distribution and localisation of activated astrocytes and Aβ plaques in the hippocampus. GFAP-labelled astrocytes (red) around Aβ plaques (green) are shown. Scale bars: 100 μm. **D** Double labelling for Iba1 (red) and Aβ (green) respectively shows the activated microglia and Aβ plaques in the hippocampus of the Tg mouse. Scale bars: 200 μm. The high-magnification images in the right panels correspond to the areas indicated in the boxes. Scale bars: 100 μm. **E** Quantification of the relative intensities of GFAP and Iba1. **F** The protein levels of GFAP, Iba1 and CD11b were examined by Western blot analysis. Blots were repeated at least three times for every condition. * $p < 0.05$, ** $p < 0.01$ and *** $p < 0.001$ vs vehicle-treated mice; ### $p < 0.001$ vs the WT mice by the one- or two-way ANOVA with post hoc Fisher's LSD tests as appropriate. Values represent the mean \pm SD. $n = 6$ in each group.



expression is elevated in the cortex of the brains from AD patients and the aged brain [25]. Wang and colleagues reported that CEBP β was significantly increased in a 3xTg-AD mouse model, which harboured the variants of the genes, Psen1 allele, APP Swedish mutation and MAPT allele. A β -plaque depositions and

hyperphosphorylated tau are observed in the hippocampus of the mouse model between 12–15 months of age. Knockout of CEBP β in this 3xTg-AD mice could reduce above AD-like pathologies *via* inhibiting δ -secretase [65]. Interestingly, CEBP β overexpression induced by hippocampal stereotactic injection with Adeno-

Fig. 6 CA-SBE β CD NPs-mediated inhibition of proinflammatory cytokines is involved in the regulation of CEBP β in the brains of APP/PS1 mice. CA-SBE β CD NPs (loaded with 10 or 30 mg/kg CA) or SBE β CD NPs (vehicle control) were administered to 4-month-old APP/PS1 Tg mice and age-matched WT C57BL/6 mice for 5 months. **A** Western blot and quantitative analysis showing the protein levels of pro- and mature IL-1 β , IL-6 and TNF α in the mouse brain. Real-time PCR analysis showing the mRNA levels of TNF α (**B**) and IL-6 (**C**). **D** Western blot analysis of NF κ B p65 expression in the cytosol and nucleus in protein lysates from Tg and WT mice brains. The protein expression levels of COX-2 and NLRP3 were analysed. Representative blots showing the protein levels of cytosolic and nuclear CEBP β . The mRNA levels of NF κ B (**E**) and CEBP β (**F**). **G** Representative images of immunofluorescence (IF) staining for CEBP β (red) and GFAP (green) in the hippocampi of WT and Tg mice. The nuclei were labelled with DAPI (blue). The white arrows indicate colocalization of CEBP β and GFAP. Scale bars: 60 μ m. The enlarged images in the right panels show GFAP- and CEBP β -positive cells. Scale bars: 10 μ m. **H** IF labelling of CEBP β and Iba1 in the hippocampus of Tg mice. Scale bars: 10 μ m. The white arrowheads indicate the colocalizations of CEBP β and Iba1. Right panels: enlarged images of the indicated cells. Scale bars: 10 μ m. **I** The interaction of CEBP β with NF κ B was assessed by Co-IP. ChIP was performed to assess the NF κ B-mediated transcription of IL-6 (**J**) and TNF α (**K**). * p < 0.05, ** p < 0.01 and *** p < 0.001 vs vehicle-treated mice; #### p < 0.001 vs the WT mice by the two-way ANOVA with post hoc Fisher's LSD tests. Values represent the mean \pm SD. n = 6 in each group. Blots were repeated at least three times for every condition.

associated virus vector-encoding CEBP β led to the upregulation of ApoE4 in this 3 \times Tg-AD mice and caused the losses of dendritic spines in the hippocampal neurons [66]. These results indicate the significance of CEBP β as a pivotal transcription factor for the genes on regulating APP processing and tau pathology in AD. Further animal experiments need to be performed to address the effects of CA-SBE β CD NPs-induced CEBP β inhibition on its other downstream targets. Knocking down CEBP β reduces NF κ B p65 subunit expression and inhibits NF κ B p65 activation, whereas silencing p65 does not affect CEBP β [20]. The interaction of NF κ B with CEBP through the bZIP region can enhance the transcriptional activity of NF κ B [24]. Upregulating CEBP β expression enhanced the binding activity of p65 to the promoter of IL-1 β ; accordingly, inhibition of CEBP β suppressed the DNA binding activity of NF κ B [20]. We propose that suppressing the abnormal increase in CEBP β expression and inhibiting the interaction of CEBP β with NF κ B might disturb the proinflammatory environment and block AD progression. In our study, we showed that CA administration ameliorated the aberrant increase in CEBP β protein expression in the Tg mice brains. CA reversed the inflammatory mediator-induced activation of CEBP β /NF κ B signalling in vitro and reduced A β secretions *via* inhibiting BACE1. These findings provide a plausible link between targeting proinflammatory cytokine transcription and inhibiting amyloidogenesis. Interestingly, our molecular docking result suggests that CA interacts with CEBP β through hydrogen bonds. The amino acid residues of CEBP β forming hydrogen bonds with CA are Asparagine-296 and Alanine-292. The binding affinity was -25.12 KJoule/mol (Supplementary Fig. S1). The results of molecular docking indicate the potential of CA on CEBP β intervention. Further studies of the postmortem brains of AD patients may help elucidate the exact effects of CEBP β on regulating NF κ B target genes during AD pathology (Fig. 9). Our results in combination with previous findings regarding the neuroprotective effects of CA [63] confirmed that CA has therapeutic potential for AD. Limitations of this study include that the molecular docking only mimics the interactions of CA and CEBP β ; the CEBP β immunostaining in the CA-treated mice brains does not provide the direct demonstration of CA on inhibiting CEBP β by CA-CEBP β interactions. Methods such as surface plasmon resonance (SPR) will allow for investigating the functional nature and kinetic information of CA-CEBP β interactions.

We packaged CA in NPs to overcome the limitations induced by the poor solubility of CA and enhance the brain bioavailability of CA. The negatively charged nanoparticles showed good blood stability, but their cellular uptake was relatively low. The positively charged nanoparticles easily interact with negatively charged blood components (plasma proteins, etc.) [67], whereas, which leads to the decrease in its stability and be eliminated from the body. It is a hot issue to prepare a delivery system with the advantages of circulation stability and higher cellular uptake. Maximising drug exposures are crucial for scientific research of

diseases. Nanoparticles may enter the cells through nonspecific internalisation such as phagocytosis, pinocytosis and endocytosis [68]. SBE β CD attracts more attention as a solubilizing excipient, especially for drugs with poor aqueous solubility. The negative charge located at a flexible butyl chain on the SBE β CD [69] may facilitate the interactions between SBE β CD and drug [70]; meanwhile, the flexible and anamorphous butyl chain endows higher molecular mobility, which might be beneficial to the drug permeation [71]. It has been reported that the SBE β CD-based delivery system could enhance the cellular uptake of inclusion complexed drugs in vitro and ex vivo [72]. The hydrophilic surface of SBE β CD forms a nanometre IC with the poorly water-soluble CA, improving the solubility of CA and preventing its uptake by the mononuclear phagocytic system [73], and improving drugs bioavailability [74, 75]. The hydrogen bonds between SBE β CD and CA make the IC more energetically stable [76]. In our study, the sizes of the NPs were evenly distributed, and the particle size was less than 100 nm; this facilitated the delivery of the NPs through the BBB [77] and prevented them from being filtered by the spleen [78]. The zeta potential (absolute value) was increased in the CA-SBE β CD NPs relative to those of the vehicle particles without CA. The results are probably due to the CA being encapsulated within the SBE β CD cavity, forming inclusion complexes through non-covalent interactions [79]. The interactions increase the density of nanostructures and enhance the stability of the nanosystem. CA-SBE β CD NPs exhibited sustained release behaviours without initial release burst at physiological conditions (pH 7.4). Meanwhile, the release behaviours were relatively stable in the acidic environment (pH 6.0), suggesting that the delivery system could overcome the barrier of the acid endosome, and enter the cells [80]. We verified the BBB permeability of the NPs in vitro and in vivo. The detailed transmembrane pattern and mechanism of SBE β CD delivery deserve further investigation.

CONCLUSIONS

Our findings show that the NPs can be used as a promising brain delivery nanosystem. Preliminary studies suggested that SBE β CD NPs are a safe and viable option for delivering CA across the BBB. A pharmacological study of the impact of CA SBE β CD NPs in an AD model demonstrated that CA exerted neuroprotective effects. Oral administration of CA SBE β CD NPs improved the cognitive function of AD mice, inhibited proinflammatory cytokine production, and alleviated neurodegenerative processes. We observed that the increase in CEBP β expression was related to the upregulation of the expression of NF κ B target genes, contributing to the impairment of the glia-associated inflammatory response. CA treatment ameliorated glia-mediated neuronal damage under chronic inflammatory conditions and reduced A β deposition *via* suppressing CEBP/NF κ B signalling pathway.

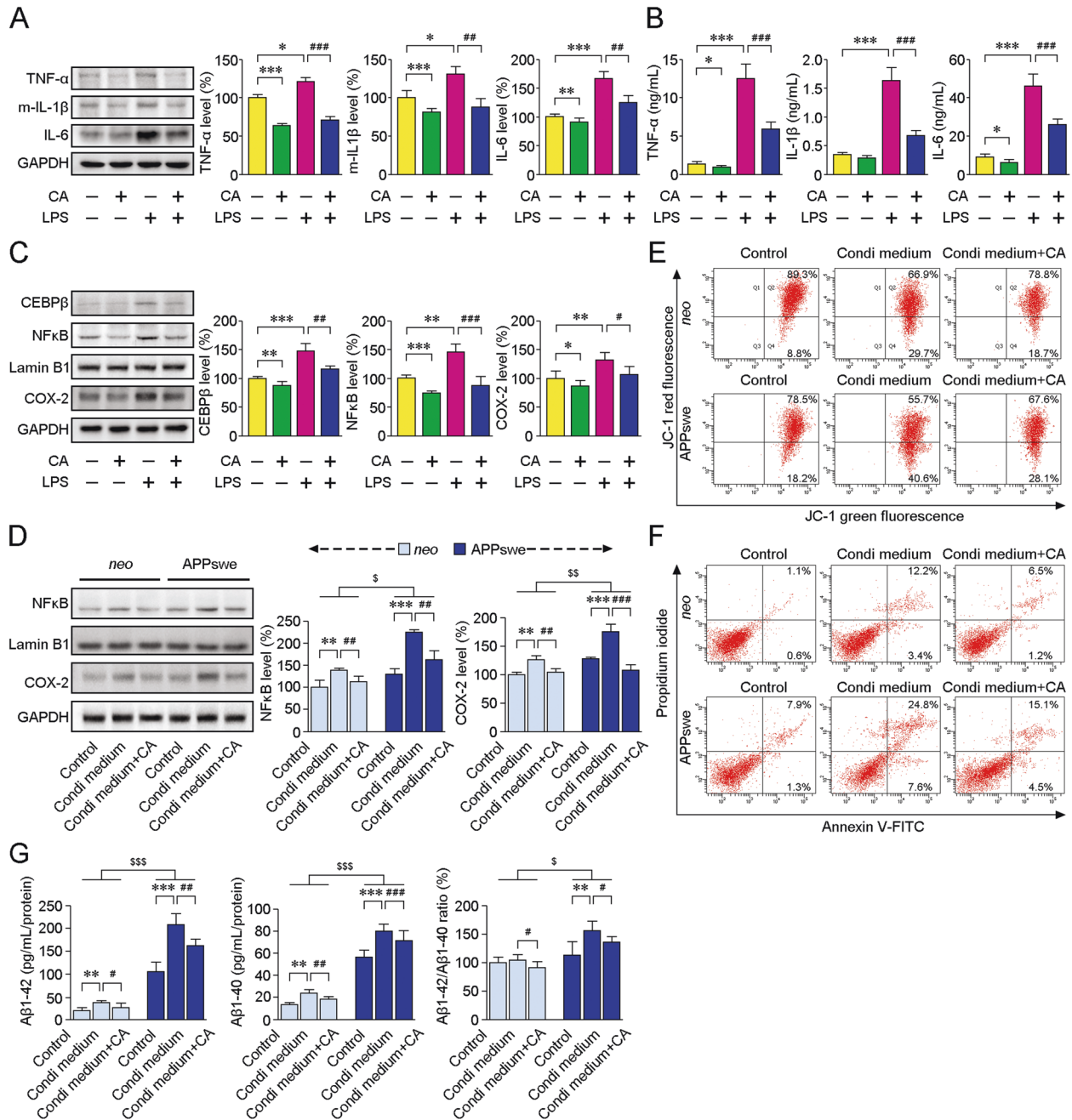


Fig. 7 CA treatment abolishes the effects of gliia-secreted proinflammatory cytokines on neuronal damage and A β secretion. A172 human glioblastoma cells were incubated with 1 μ g/mL LPS for 24 h to trigger proinflammatory responses and then treated with CA at a final concentration of 1 μ M for 12 h. **A** Western blot analysis was performed to evaluate the protein expression of IL-1 β , IL-6 and TNF α . **B** The secretion of IL-1 β , IL-6 and TNF α was measured by ELISA. **C** Representative blots showing the protein levels of COX-2, nuclear CEBP β and NF κ B in A172 cells. **D** SH-SY5Y cells overexpressing human APPsw or empty vector (*neo*) were cultured in LPS-primed cell-conditioned medium and treated with or without CA. The protein levels of nuclear NF κ B and COX-2 were measured. **E** The mitochondrial transmembrane potential of APPsw and *neo* cells was determined by FCM. The percent of red and green fluorescence signal of JC-1 was measured to assess the degree of mitochondrial depolarisation. **F** Apoptosis of APPsw and *neo* cells were labelled by Annexin V-FITC/PI staining and analysed by FCM. **G** The secretion of A β 40 and A β 42 by APPsw and *neo* cells was measured by ELISA. The ratio of A β 42 to A β 40 was quantified. The data were representative of at least three independent experiments. * p < 0.05, ** p < 0.01 and *** p < 0.001 vs untreated cells; # p < 0.05, ## p < 0.01 and ### p < 0.001 vs the LPS-stimulated group (A–C). ** p < 0.01 and *** p < 0.001 vs the group treated with the medium of A172 cells not incubated with LPS (Control); # p < 0.05, ## p < 0.01 and ### p < 0.001 vs the group incubated with the medium of LPS-primed A172 cells without CA treatment; $\$$ p < 0.05, $\$\$$ p < 0.01 and $\$\$\$$ p < 0.001 vs *neo* cells (D, G). Data were submitted to two-way ANOVA with Fisher LSD post hoc tests. Values represent the mean \pm SD. All experiments were repeated at least three times.

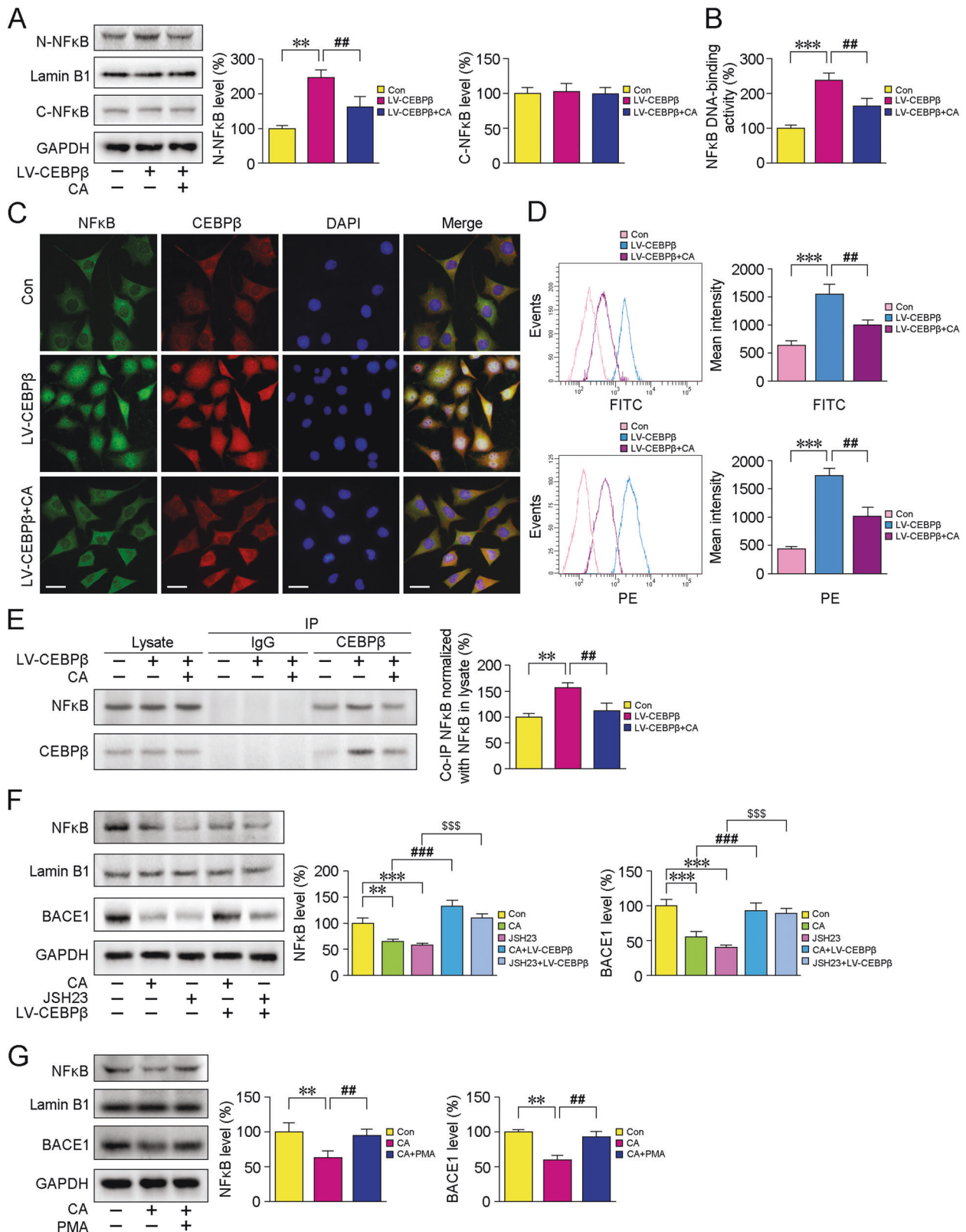


Fig. 8 CA-mediated inhibition of CEBPβ/NFκB signalling directly inhibits BACE1. **A** Representative blots of NFκB p65 in SH-SY5Y cells following transfection with a lentiviral vector-encoding human CEBPβ (LV-CEBPβ) or treatment with LV-CEBPβ plus CA. **B** The DNA binding activity of NFκB p65 was determined by ELISA. **C** IF staining shows the NFκB p65 (green) and CEBPβ (red) protein expressions. Scale bars: 20 μm. **D** FCM analysis of NFκB p65 (FITC channel) and CEBPβ (PE channel) after treatment with LV-CEBPβ or LV-CEBPβ plus CA. **E** The binding of CEBPβ to NFκB was examined by Co-IP. **F** Similar to JSH-23, CA treatment-induced decreases in nuclear NFκB p65 and cytosolic BACE1 expressions were blocked by LV-CEBPβ. **G** CA-mediated inhibition of BACE1 was diminished by the NFκB activator, PMA. The data were representative of at least three independent experiments. ** $p < 0.01$ and *** $p < 0.001$ vs the controls; ## $p < 0.01$ vs the LV-CEBPβ-treated group (A–E). ** $p < 0.01$ and *** $p < 0.001$ vs the controls; ### $p < 0.001$ versus CA-treated group; \$\$\$ $p < 0.001$ versus JSH-23 treatment group (F). ** $p < 0.01$ vs the controls; ## $p < 0.01$ vs the CA treatment group (G). Data were analysed using one-way ANOVA and Fisher LSD post hoc tests. Values represent the mean \pm SD of at least three independent experiments.

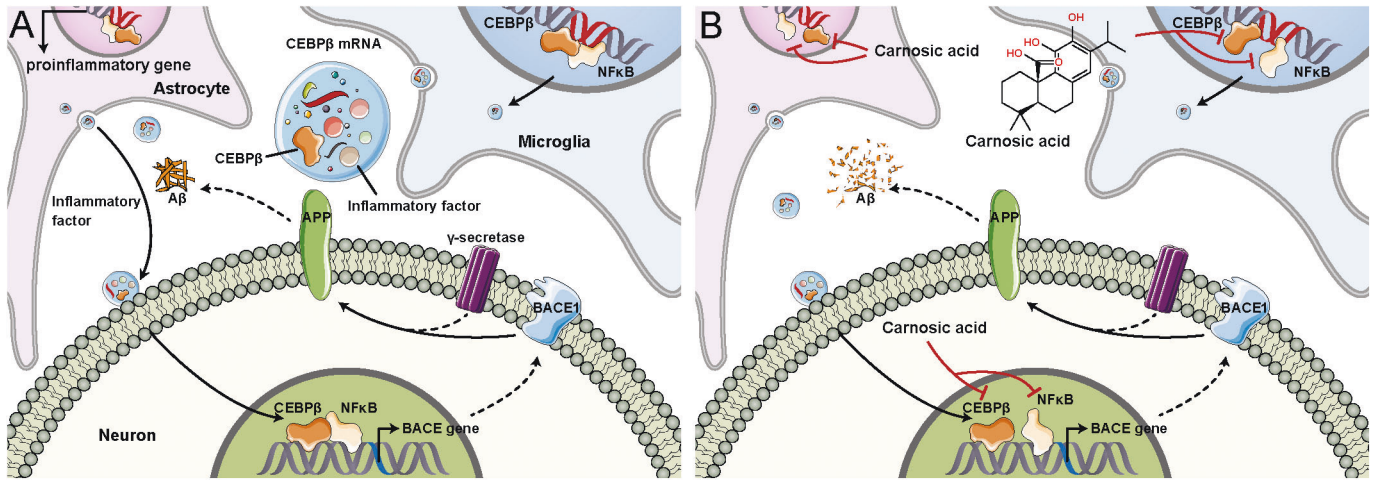


Fig. 9 Schematic diagram of CA on the regulation of CEBPβ–NFκB interaction in the AD brain. A The increases of CEBPβ–NFκB interaction enhance NFκB DNA binding activity, facilitating the transcription of NFκB target genes. The upregulation of CEBPβ and NFκB downstream genes, proinflammatory cytokines, could increase the releases of inflammatory factor from the microbubbles or exosomes secreted by microglia or astrocytes. NFκB-mediated increases and activation of BACE1 prompt the amyloidogenic processing of APP, followed by the γ -secretase cleavage, leading to the A β production by the neuron. Chronic inflammatory conditions and A β depositions exacerbate the binding of CEBPβ–NFκB, deteriorating the AD-like pathology. **B** CA provides neuroprotective effects by preventing the nucleus translocation of NFκB, reducing the expressions of proinflammatory cytokines. Meanwhile, CA reduces the CEBPβ–NFκB interaction and alleviates A β aggregation via inhibiting the amyloidogenic proteolytic pathway of APP.

DATA AVAILABILITY

Original western blots information is shown in Supplementary Figs. S2–S5. The datasets used and/or analysed in the present study are available from the corresponding authors.

REFERENCES

- Swardfager W, Lanctot K, Rothenburg L, Wong A, Cappell J, Herrmann N. A meta-analysis of cytokines in Alzheimer's disease. *Biol Psychiatry*. 2010;68:930–41.
- Too LK, Hunt N, Simunovic MP. The role of inflammation and infection in age-related neurodegenerative diseases: lessons from bacterial meningitis applied to Alzheimer disease and age-related macular degeneration. *Front Cell Neurosci*. 2021;15:635486.
- Griffin WS, Stanley LC, Ling C, White L, MacLeod V, Perrot LJ, et al. Brain interleukin 1 and S-100 immunoreactivity are elevated in Down syndrome and Alzheimer disease. *Proc Natl Acad Sci USA*. 1989;86:7611–5.
- Hull M, Berger M, Volk B, Bauer J. Occurrence of interleukin-6 in cortical plaques of Alzheimer's disease patients may precede transformation of diffuse into neuritic plaques. *Ann N Y Acad Sci*. 1996;777:205–12.
- van der Wal EA, Gomez-Pinilla F, Cotman CW. Transforming growth factor-beta 1 is in plaques in Alzheimer and Down pathologies. *Neuroreport*. 1993;4:69–72.
- Tarkowski E, Andreasen N, Tarkowski A, Blennow K. Intrathecal inflammation precedes development of Alzheimer's disease. *J Neurol Neurosurg Psychiatry*. 2003;74:1200–5.
- Brosseron F, Krauthausen M, Kummer M, Heneka MT. Body fluid cytokine levels in mild cognitive impairment and Alzheimer's disease: a comparative overview. *Mol Neurobiol*. 2014;50:534–44.
- Heneka MT, Golenbock DT, Latz E. Innate immunity in Alzheimer's disease. *Nat Immunol*. 2015;16:229–36.
- Ritzel RM, Patel AR, Pan S, Crapser J, Hammond M, Jellison E, et al. Age- and location-related changes in microglial function. *Neurobiol Aging*. 2015;36:2153–63.
- Quintanilla RA, Orellana DI, Gonzalez-Billault C, Maccioni RB. Interleukin-6 induces Alzheimer-type phosphorylation of tau protein by deregulating the cdk5/p35 pathway. *Exp Cell Res*. 2004;295:245–57.
- Krstic D, Madhusudan A, Doehner J, Vogel P, Notter T, Imhof C, et al. Systemic immune challenges trigger and drive Alzheimer-like neuropathology in mice. *J Neuroinflammation*. 2012;9:151.
- Bolos M, Llorens-Martin M, Perea JR, Jurado-Arjona J, Rabano A, Hernandez F, et al. Absence of CX3CR1 impairs the internalization of Tau by microglia. *Mol Neurodegener*. 2017;12:59.
- McGeer PL, McGeer E, Rogers J, Sibley J. Anti-inflammatory drugs and Alzheimer disease. *Lancet*. 1990;335:1037.
- Gupta PP, Pandey RD, Jha D, Shrivastav V, Kumar S. Role of traditional non-steroidal anti-inflammatory drugs in Alzheimer's disease: a meta-analysis of randomized clinical trials. *Am J Alzheimers Dis Other Dement*. 2015;30:178–82.
- de Jong D, Jansen R, Hoefnagels W, Jellesma-Eggenkamp M, Verbeek M, Borm G, et al. No effect of one-year treatment with indomethacin on Alzheimer's disease progression: a randomized controlled trial. *PLoS ONE*. 2008;3:e1475.
- Jaturapatporn D, Isaac MG, McCleery J, Tabet N. Aspirin, steroidal and non-steroidal anti-inflammatory drugs for the treatment of Alzheimer's disease. *Cochrane Database Syst Rev*. 2012;CD006378.
- Frezza RL, Lourenco MV, De, Felice FG. Challenges for Alzheimer's disease therapy: insights from novel mechanisms beyond memory defects. *Front Neurosci*. 2018;12:37.
- Butchart J, Brook L, Hopkins V, Teeling J, Puntener U, Culliford D, et al. Etanercept in Alzheimer disease: a randomized, placebo-controlled, double-blind, phase 2 trial. *Neurology* 2015;84:2161–8.
- Fonseca GJ, Seidman JS, Glass CK. Genome-wide approaches to defining macrophage identity and function. *Microbiol Spectr*. 2016;4. <https://doi.org/10.1128/microbiolspec.MCHD-0039-2016>.
- Ma J, Liu C, Yang Y, Yu J, Yang J, Yu S, et al. C/EBPbeta acts upstream of NF-kappaB P65 subunit in Ox-LDL-induced IL-1beta production by macrophages. *Cell Physiol Biochem*. 2018;48:1605–15.
- Papin S, Cazeneuve C, Duquesnoy P, Jeru I, Sahali D, Amselem S. The tumor necrosis factor alpha-dependent activation of the human mediterranean fever (MEFV) promoter is mediated by a synergistic interaction between C/EBP beta and NF kappaB p65. *J Biol Chem*. 2003;278:48839–47.
- Straccia M, Gresa-Arribas N, Dentesano G, Ejarque-Ortiz A, Tusell JM, Serratos J, et al. Pro-inflammatory gene expression and neurotoxic effects of activated microglia are attenuated by absence of CCAAT/enhancer binding protein beta. *J Neuroinflammation*. 2011;8:156.
- Morales-Garcia JA, Gine E, Hernandez-Encinas E, Aguilar-Morante D, Sierra-Magro A, Sanz-SanCristobal M, et al. CCAAT/enhancer binding protein beta silencing mitigates glial activation and neurodegeneration in a rat model of Parkinson's disease. *Sci Rep*. 2017;7:13526.
- Stein B, Cogswell PC, Baldwin AS Jr. Functional and physical associations between NF-kappa B and C/EBP family members: a Rel domain-bZIP interaction. *Mol Cell Biol*. 1993;13:3964–74.
- Strohmeier R, Shelton J, Lougheed C, Breitkopf T. CCAAT-enhancer binding protein-beta expression and elevation in Alzheimer's disease and microglial cell cultures. *PLoS ONE*. 2014;9:e86617.
- Srinivasan K, Friedman BA, Larson JL, Lauffer BE, Goldstein LD, Appling LL, et al. Untangling the brain's neuroinflammatory and neurodegenerative transcriptional responses. *Nat Commun*. 2016;7:11295.
- Wang ZH, Gong K, Liu X, Zhang Z, Sun X, Wei ZZ, et al. C/EBPbeta regulates delta-secretase expression and mediates pathogenesis in mouse models of Alzheimer's disease. *Nat Commun*. 2018;9:1784.
- Kim YJ, Kim JS, Seo YR, Park JH, Choi MS, Sung MK. Carnosic acid suppresses colon tumor formation in association with anti-dipogenic activity. *Mol Nutr Food Res*. 2014;58:2274–85.

29. Liu M, Zhou X, Zhou L, Liu Z, Yuan J, Cheng J, et al. Carnosic acid inhibits inflammation response and joint destruction on osteoclasts, fibroblast-like synoviocytes, and collagen-induced arthritis rats. *J Cell Physiol.* 2018;233:6291–303.
30. Xie Z, Zhong L, Wu Y, Wan X, Yang H, Xu X, et al. Carnosic acid improves diabetic nephropathy by activating Nrf2/ARE and inhibition of NF-kappaB pathway. *Phytomedicine* 2018;47:161–73.
31. Li Y, Lin S, Liu P, Huang J, Qiu J, Wen Z, et al. Carnosol suppresses RANKL-induced osteoclastogenesis and attenuates titanium particles-induced osteolysis. *J Cell Physiol.* 2021;236:1950–66.
32. Mrak RE, Griffin WS. Glia and their cytokines in progression of neurodegeneration. *Neurobiol Aging.* 2005;26:349–54.
33. Jain AS, Date AA, Pissurlenkar RR, Coutinho EC, Nagarsenker MS. Sulfobutyl ether (7) beta-cyclodextrin (SBE(7) beta-CD) carbamazepine complex: preparation, characterization, molecular modeling, and evaluation of in vivo anti-epileptic activity. *AAPS PharmSciTech.* 2011;12:1163–75.
34. Wang CY, Wang ZY, Xie JW, Wang T, Wang X, Xu Y, et al. Di-3-n-butylphthalide-induced upregulation of antioxidant defense is involved in the enhancement of cross talk between CREB and Nrf2 in an Alzheimer's disease mouse model. *Neurobiol Aging.* 2016;38:32–46.
35. Hurttila H, Koponen JK, Kansanen E, Jyrkkanen HK, Kivela A, Kylvatie R, et al. Oxidative stress-inducible lentiviral vectors for gene therapy. *Gene Ther.* 2008;15:1271–9.
36. Loftsson T, Duchene D. Cyclodextrins and their pharmaceutical applications. *Int J Pharm.* 2007;329:1–11.
37. Hong S, Beja-Glasser VF, Nfonoyim BM, Frouin A, Li S, Ramakrishnan S, et al. Complement and microglia mediate early synapse loss in Alzheimer mouse models. *Science.* 2016;352:712–6.
38. Chen F, Jiang G, Liu H, Li Z, Pei Y, Wang H, et al. Melatonin alleviates intervertebral disc degeneration by disrupting the IL-1beta/NF-kappaB-NLRP3 inflammasome positive feedback loop. *Bone Res.* 2020;8:10.
39. Rahman SM, Baquero KC, Choudhury M, Janssen RC, de la Houssaye BA, Sun M, et al. C/EBPbeta in bone marrow is essential for diet induced inflammation, cholesterol balance, and atherosclerosis. *Atherosclerosis* 2016;250:172–9.
40. Marwarha G, Schommer J, Lund J, Schommer T, Ghribi O. Palmitate-induced C/EBP homologous protein activation leads to NF-kappaB-mediated increase in BACE1 activity and amyloid beta genesis. *J Neurochem.* 2018;144:761–79.
41. Ferretti MT, Bruno MA, Ducatenzeiler A, Klein WL, Cuervo AC. Intracellular Abeta-oligomers and early inflammation in a model of Alzheimer's disease. *Neurobiol Aging.* 2012;33:1329–42.
42. Vasto S, Candore G, Balistreri CR, Caruso M, Colonna-Romano G, Grimaldi MP, et al. Inflammatory networks in ageing, age-related diseases and longevity. *Mech Ageing Dev.* 2007;128:83–91.
43. Condello C, Yuan P, Schain A, Grutzendler J. Microglia constitute a barrier that prevents neurotoxic protofibrillar Abeta42 hotspots around plaques. *Nat Commun.* 2015;6:6176.
44. Ross FM, Allan SM, Rothwell NJ, Verkhratsky A. A dual role for interleukin-1 in LTP in mouse hippocampal slices. *J Neuroimmunol.* 2003;144:61–67.
45. Stellwagen D, Malenka RC. Synaptic scaling mediated by glial TNF-alpha. *Nature* 2006;440:1054–9.
46. Czirr E, Wyss-Coray T. The immunology of neurodegeneration. *J Clin Invest.* 2012;122:1156–63.
47. Franceschi C, Campisi J. Chronic inflammation (inflammaging) and its potential contribution to age-associated diseases. *J Gerontol A Biol Sci Med Sci.* 2014;69:54–9.
48. Krabbe G, Halle A, Matyash V, Rinnenthal JL, Eom GD, Bernhardt U, et al. Functional impairment of microglia coincides with Beta-amyloid deposition in mice with Alzheimer-like pathology. *PLoS ONE.* 2013;8:e60921.
49. Hickman SE, Allison EK, El Khoury J. Microglial dysfunction and defective beta-amyloid clearance pathways in aging Alzheimer's disease mice. *J Neurosci.* 2008;28:8354–60.
50. Shih RH, Wang CY, Yang CM. NF-kappaB signaling pathways in neurological inflammation: a mini review. *Front Mol Neurosci.* 2015;8:77.
51. Kabe Y, Ando K, Hirao S, Yoshida M, Handa H. Redox regulation of NF-kappaB activation: distinct redox regulation between the cytoplasm and the nucleus. *Antioxid Redox Signal.* 2005;7:395–403.
52. Engelmann C, Haenold R. Transcriptional control of synaptic plasticity by transcription factor NF-kappaB. *Neural Plast.* 2016;2016:7027949.
53. Patel JR, Brewer GJ. Age-related differences in NFkappaB translocation and Bcl-2/Bax ratio caused by TNFalpha and Abeta42 promote survival in middle-age neurons and death in old neurons. *Exp Neurol.* 2008;213:93–100.
54. Nonaka M, Chen XH, Pierce JE, Leoni MJ, McIntosh TK, Wolf JA, et al. Prolonged activation of NF-kappaB following traumatic brain injury in rats. *J Neurotrauma.* 1999;16:1023–34.
55. Mattson MP, Camandola S. NF-kappaB in neuronal plasticity and neurodegenerative disorders. *J Clin Invest.* 2001;107:247–54.
56. Tsay HJ, Huang YC, Huang FL, Chen CP, Tsai YC, Wang YH, et al. Amyloid beta peptide-mediated neurotoxicity is attenuated by the proliferating microglia more potently than by the quiescent phenotype. *J Biomed Sci.* 2013;20:78.
57. Mu Y, Zhang Y, Wu J, Li Q. NLR5 attenuates inflammatory response in IL-1beta-stimulated human osteoarthritis chondrocytes through the NF-kappaB signaling pathway. *Aging.* 2021;13:20651–60.
58. Wang R, Chen S, Liu Y, Diao S, Xue Y, You X, et al. All-trans-retinoic acid reduces BACE1 expression under inflammatory conditions via modulation of nuclear factor kappaB (NFkappaB) signaling. *J Biol Chem.* 2015;290:22532–42.
59. Shakibaei M, John T, Schulze-Tanzil G, Lehmann I, Mobasheri A. Suppression of NF-kappaB activation by curcumin leads to inhibition of expression of cyclo-oxygenase-2 and matrix metalloproteinase-9 in human articular chondrocytes: Implications for the treatment of osteoarthritis. *Biochem Pharm.* 2007;73:1434–45.
60. Zhang H, Li YY, Wu XZ. Effect of Tetrandrine on LPS-induced NF-kappaB activation in isolated pancreatic acinar cells of rat. *World J Gastroenterol.* 2006;12:4232–1236.
61. Liu Y, Zhang Y, Hu M, Li YH, Cao XH. Carnosic acid alleviates brain injury through NFkappaB-regulated inflammation and Caspase3-associated apoptosis in high fat-induced mouse models. *Mol Med Rep.* 2019;20:495–504.
62. de Oliveira MR. Carnosic acid as a promising agent in protecting mitochondria of brain cells. *Mol Neurobiol.* 2018;55:6687–99.
63. Meng P, Yoshida H, Tanji K, Matsumiya T, Xing F, Hayakari R, et al. Carnosic acid attenuates apoptosis induced by amyloid-beta 1-42 or 1-43 in SH-SY5Y human neuroblastoma cells. *Neurosci Res.* 2015;94:1–9.
64. Matsumoto M, Sakao Y, Akira S. Inducible expression of nuclear factor IL-6 increases endogenous gene expression of macrophage inflammatory protein-1 alpha, osteopontin and CD14 in a monocytic leukemia cell line. *Int Immunol.* 1998;10:1825–35.
65. Wang H, Liu X, Chen S, Ye K. Spatiotemporal activation of the C/EBPbeta/delta-secretase axis regulates the pathogenesis of Alzheimer's disease. *Proc Natl Acad Sci USA.* 2018;115:E12427–E12434.
66. Xia Y, Wang ZH, Zhang J, Liu X, Yu SP, Ye KX, et al. C/EBPbeta is a key transcription factor for ApoE and preferentially mediates ApoE4 expression in Alzheimer's disease. *Mol Psychiatry.* 2020. <https://doi.org/10.1038/s41380-020-00956-4>.
67. Frohlich E. The role of surface charge in cellular uptake and cytotoxicity of medical nanoparticles. *Int J Nanomed.* 2012;7:5577–91.
68. Ma N, Ma C, Li C, Wang T, Tang Y, Wang H, et al. Influence of nanoparticle shape, size, and surface functionalization on cellular uptake. *J Nanosci Nanotechnol.* 2013;13:6485–98.
69. Fulop Z, Saokham P, Loftsson T. Sulfobutylether-beta-cyclodextrin/chitosan nano- and microparticles and their physicochemical characteristics. *Int J Pharm.* 2014;472:282–7.
70. Zia V, Rajewski RA, Stella VJ. Effect of cyclodextrin charge on complexation of neutral and charged substrates: comparison of (SBE)7M-beta-CD to HP-beta-CD. *Pharm Res.* 2001;18:667–73.
71. Mohandoss S, Atchudan R, Immanuel Edison TNJ, Mandal TK, Palanisamy S, You S, et al. Enhanced solubility of guanosine by inclusion complexes with cyclodextrin derivatives: Preparation, characterization, and evaluation. *Carbohydr Polym.* 2019;224:115166.
72. Kumar R, Sinha VR, Dahiya L, Singh G, Sarwal A. Impact of cyclodextrin derivatives on systemic release of duloxetine HCl via buccal route. *Drug Dev Ind Pharm.* 2020;46:931–45.
73. Owens DE 3rd, Peppas NA. Opsonization, biodistribution, and pharmacokinetics of polymeric nanoparticles. *Int J Pharm.* 2006;307:93–102.
74. Wang Z, Li Y. Raloxifene/SBE-beta-CD inclusion complexes formulated into nanoparticles with chitosan to overcome the absorption barrier for bioavailability enhancement. *Pharmaceutics* 2018;10:76.
75. Zhu W, Wu J, Guo X, Sun X, Li Q, Wang J, et al. Development and physicochemical characterization of chitosan hydrochloride/sulfobutyl ether-beta-cyclodextrin nanoparticles for cinnamaldehyde entrapment. *J Food Biochem.* 2020;44:e13197.
76. van de Manakker F, Vermonden T, van Nostrum CF, Hennink WE. Cyclodextrin-based polymeric materials: synthesis, properties, and pharmaceutical/biomedical applications. *Biomacromolecules.* 2009;10:3157–75.
77. Lu W, Zhang Y, Tan YZ, Hu KL, Jiang XG, Fu SK. Cationic albumin-conjugated pegylated nanoparticles as novel drug carrier for brain delivery. *J Control Release.* 2005;107:428–48.
78. Zhao ZX, Gao SY, Wang JC, Chen CJ, Zhao EY, Hou WJ, et al. Self-assembly nanomicelles based on cationic mPEG-PLA-b-Polyarginine(R15) triblock copolymer for siRNA delivery. *Biomaterials.* 2012;33:6793–807.
79. Tan S, Ladewig K, Fu Q, Blencowe A, Qiao GG. Cyclodextrin-based supramolecular assemblies and hydrogels: recent advances and future perspectives. *Macromol Rapid Commun.* 2014;35:1166–84.

80. Hinde E, Thammasiraphop K, Duong HT, Yeow J, Karagoz B, Boyer C, et al. Pair correlation microscopy reveals the role of nanoparticle shape in intracellular transport and site of drug release. *Nat Nanotechnol.* 2017;12:81–89.

ACKNOWLEDGEMENTS

Sample processing and imaging of TEM were conducted in the Electron microscope centre of the Molecular Cell Biology Department at China Medical University.

AUTHOR CONTRIBUTIONS

WC-Y and XY performed the study concept and design, review and revision of the paper; WY-B, LX, YB and ZQ performed the development of methodology and writing; JF-T and WM provided acquisition, analysis and interpretation of data and the statistical analysis; ZX, KL, LY, SP and GY provided technical and material support. All authors read and approved the final paper.

FUNDING

This work was supported by the National Natural Science Foundation of China (Nos. 81971026 and 81671041), Natural Science Foundation of Liaoning Provincial Science & Technology Department in China (No. 2018225086), Natural Science Foundation of Jilin Provincial Educational Department in China (No. JJKH20200455KJ).

COMPETING INTERESTS

The authors declare no competing interests.

ADDITIONAL INFORMATION

Supplementary information The online version contains supplementary material available at <https://doi.org/10.1038/s41419-022-04765-1>.

Correspondence and requests for materials should be addressed to Xu Ye or Wang Chun-Yan.

Reprints and permission information is available at <http://www.nature.com/reprints>

Publisher's note Springer Nature remains neutral with regard to jurisdictional claims in published maps and institutional affiliations.



Open Access This article is licensed under a Creative Commons Attribution 4.0 International License, which permits use, sharing, adaptation, distribution and reproduction in any medium or format, as long as you give appropriate credit to the original author(s) and the source, provide a link to the Creative Commons license, and indicate if changes were made. The images or other third party material in this article are included in the article's Creative Commons license, unless indicated otherwise in a credit line to the material. If material is not included in the article's Creative Commons license and your intended use is not permitted by statutory regulation or exceeds the permitted use, you will need to obtain permission directly from the copyright holder. To view a copy of this license, visit <http://creativecommons.org/licenses/by/4.0/>.

© The Author(s) 2022